CHEMISTRY OF MATERIALS

ARTICLE

pubs.acs.org/cm

Very Large Silacylic Substituent Effects on Response in Silole-Based Polymer Transistors

Hui Huang,[†] Jangdae Youn,[†] Rocio Ponce Ortiz,[†,‡] Yan Zheng,[§] Antonio Facchetti,[*,†,§] and Tobin Marks[*,†]

[†]Department of Chemistry and the Materials Research Center, Northwestern University, 2145 Sheridan Road, Evanston, Illinois, 60208.

[‡]Department of Physical Chemistry, University of Málaga, Malaga, 29071, Spain.

[§]Polyera Corporation, 8045 Lamon Avenue, Skokie, Illinois, 60077, USA.

ABSTRACT: Understanding the interrelationships between molecular structure and organic thin film transistor performance is key to the realization of novel organic semiconductors achieving superior device characteristics. Herein we report the synthesis, characterization, and charge-transporting properties in organic field-effect transistors (OFETs) of dithieno silole-based oligomers and copolymers having silacycloalkyl substituents. Silacyclization of the alkyl substituents on the silole silicon atom reduces steric encumbrance, contracts solid state intermolecular $\pi-\pi$ contacts, and enhances the charge-transport capacity of the oligomers. Oligomer 3,3′-dihexylsilylene-2,2′:5,2″:5′,2‴:5″,2⁗:5‴,2⁗′-sexithiophene (**SM5**) with two Si-*n*-hexyl substituents is not FET-active, while the mobilities of 3,3′-cyclopentanylsilylene-2,2′:5,2″:5′,2‴:5″,2⁗:5‴,2⁗′-sexithiophene (**SM4**) and 3,3′-cyclobutysilylene-2,2′:5,2″:5′,2‴:5″,2⁗:5‴,2⁗′-sexithiophene (**SM3**) FETs are 2.6×10^{-4} and 3.4×10^{-4} cm^2/(V s), respectively. Single crystal structural data and melting point derived intermolecular packing trends parallel these FET results. Copolymers **P1**-**P4** based on the same dithienosilole cycloalkyl cores exhibit optimized hole mobilities of 2×10^{-5}, 6×10^{-4}, 3×10^{-4}, and 2×10^{-3} cm^2/V·s, respectively, lower than that of analogous silole-containing polymers with long Si-alkyl substituents, implying that the solubilizing and self-assembly functions of Si-alkyl substituents are important for optimizing the mobility. Interestingly, copolymer [poly{[N,N′-bis(2-octyl-dodecyl)-1,4,5,8-naphthalenedicarboximide-2,6-diyl]-*alt*-5,5′-(3,3′-cyclopentanylsilylene-2,2′-bithiophene (**P5**) films are the most ordered and exhibit a good electron mobility of 4×10^{-3} cm^2/V·s after thermal annealing. All of these OFETs exhibit good ambient-stability, which is attributed to their low-lying HOMOs (>0.2 eV lower than that of **P3HT**), a consequence of introducing silole cores into polythiophene backbones.

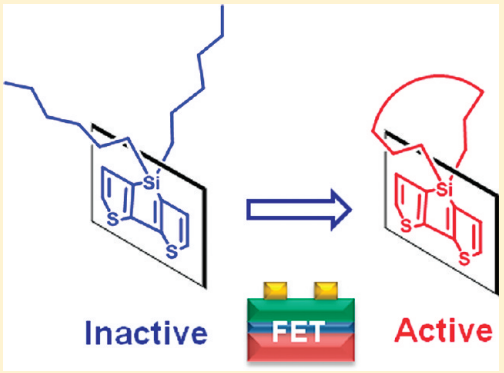

KEYWORDS: transistors, conjugated polymers, spiro siloles, sexithiophenes

INTRODUCTION

Over the past few decades, several classes of π-conjugated organic molecular and polymeric materials have been developed as semiconductors for low-cost organic electronics applications, such as organic thin-film transistors (OTFTs),[1−8] light-emitting diodes (OLEDs),[9,10] and photovoltaics (OPVs).[11−14] OTFTs are essential elements of printed integrated circuits, operating RF-ID tags, and sensors, as well as pixel drivers for active matrix displays. Among the organic semiconductors used for OTFTs, (oligo, poly)-thiophenes have been extensively investigated due to their synthetic accessibility and acceptable charge carrier mobilities (μ). For example, the oligothiophene α-sexithiophene (α-6T) was discovered as a hole transporting material in 1988,[15] and one year later thermally evaporated α-6T thin films were used to fabricate p-type OTFTs exhibiting a hole mobility of $\sim 1 \times 10^{-2}$ to 1×10^{-3} cm^2/(V s).[16,17] When electron-withdrawing groups such as perfluoroalkyl chains or perfluoroaromatic rings are introduced into the semiconductor skeleton, high-performance electron-transporting oligothiophenes were realized, which can be used to fabricate organic complementary circuits.[18−20] Unfortunately, OTFTs based on simple oligothiophenes typically exhibit low mobilities when the semiconductor films are deposited from solution, presumably due to reduced long-range structural order within the films.[21] In principle, however, thiophene-based polymers are excellent candidate materials for solution processing methodologies such as spin-coating,[22] stamping,[23] and inkjet printing[24] because of their great structural versatility and synthetic accessibility. Among polythiophenes, regioregular polythiophenes such as poly(3-hexylthiophene) (P3HT) and variants thereof are the most commonly used in OTFTs.[25−27]

Conjugated silole-containing materials have attracted great attention because of their unique electronic structures, characterized by a low-lying lowest unoccupied molecular orbital (LUMO) and a relatively small band gap resulting from the interaction between the silicon σ^* orbital and the π^* orbital of the butadiene moiety.[28−33] Furthermore, the silicon atom stabilizes the highest occupied molecular orbital (HOMO) compared to the carbon counterparts,[34] which should enhance the ambient stability of silole-containing

Received: January 3, 2011
Revised: March 1, 2011
Published: March 23, 2011

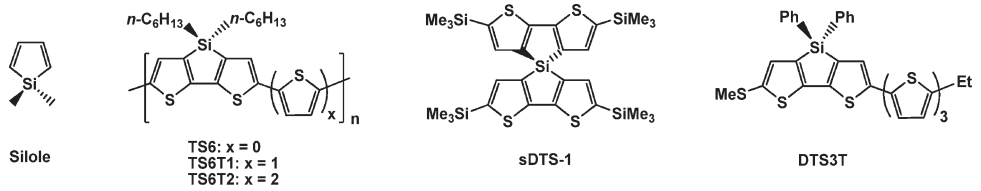

Figure 1. Structures of silole-thiophene polymers.

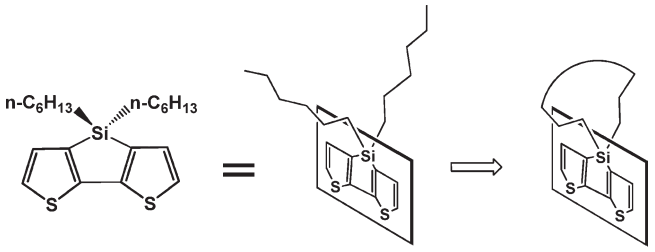

Figure 2. Strategy of replacing linear alkyl substituents with more compact spiro-cycloalkyl substituents.

polymer with respect to O_2 oxidation. Inspired by these properties, several groups have developed silole-containing small molecules, oligomers, and polymers as active materials in OLEDs,[31,35−37] OPVs,[38−42] and OTFTs.[43−47]

To enable solution-processable polymeric semiconductors, long linear[48,49] or branched alkyl[50−52] chains have been productively appended to the conjugated backbones. Furthermore, the intermolecular self-assembly of the alkyl side chains can assist in the formation of lamellar-ordered solid-state structures, strongly enhancing intermolecular charge transporting properties.[53,54] For some oligothiophenes, it is known that α,ω-core functionalization with alkyl chains also enhances carrier mobility because of improved molecular packing caused by lipophilic interactions among the alkyl chains.[55,56] On the other hand, alkyl chains connected to sp^3-hybridized bridgehead carbon or silicon atoms, such as in fluorene and silole-containing polymers, extend perpendicular to the planar polymer backbone and hinder close solid state $\pi-\pi$ stacking, hence compromise charge-transporting capacity.[57,58] The carrier mobility in organic field-effect transistors (OFETs) is generally found to increase with decreasing interplanar distances in semiconductor crystals because of greater $\pi-\pi$ orbital overlap between neighboring molecules, thus facilitating charge transfer.[59] For these reasons, replacing the bulky phenyl substituents on the dithienosilole Si atom with less bulky alkyl substituents reduces the intermolecular distances in the solid state and increases the charge transporting capacity.[60,61] Recently, we reported dithienosilole and dibenzosilole-based polymers functionalized with linear alkyl chains as the active layers to fabricate OTFTs exhibiting hole mobilities $\sim 1 \times 10^{-3} - 0.08$ $cm^2\ V^{-1}\ s^{-1}$ (Figure 1).[46] The linear alkyl chains bonded to the sp^3 silicon center are oriented perpendicular to the silole planes, conferring solubility to the silole-containing polymers. Nevertheless, the long alkyl chains appear to hinder close intermolecular $\pi-\pi$ stacking of the polymer backbones, and thus only moderate p-type mobility is achieved.

In this contribution, we report the synthesis and characterization of new molecular and polymeric semiconductors based on dithienosilole cycloalkyl cores (Figure 2). Silacyclization of the alkyl substituents on the silicon atom should reduce steric demands, contract solid state intermolecular contacts, and facilitate charge transport capacity (Figures 3 and 4). Thus, silole polymers having different-sized cycloalkyl substituents are investigated here and the solution and solid state properties of these materials compared/contrasted with those of analogous linear alkyl chain-substituted silole-thiophene derivatives. It will be seen that silicon substituent annellation results in a new series of semiconducting oligomers with significantly enhanced FET mobilities, however, the effect on the corresponding copolymers charge-transport characteristics vary considerably depending on the comonomer nature.

RESULTS AND DISCUSSION

In the following sections we first discuss the synthesis of the small molecules and polymers, followed by thermal properties, optical properties, and electrochemical characterization of the semiconductors prepared in this study. This presentation is followed by analysis of the thin film microstructure and morphology in order to understand OTFT performance. Finally, the fabrication and characterization of these devices is presented and trends analyzed.

Materials Synthesis. The new cycloalkyl silole-containing building blocks **3**, **4**, and **5** were prepared according to Scheme 1. Bithiophene was first tetrabrominated to give 3,5,3′,5′-tetrabromobithiophene, followed by selective debromination with Zn to afford 3,3′-dibromobithiophene.[46] Next, double lithiation of 3,3′-dibromobithiophene with *n*-BuLi, followed by subsequent quenching with the corresponding dichlorocycloalkylsilane, yields monomers **3**−**5** as light-yellow oils in 46−60% yield.

The reaction of compound **3** with NBS afforded an unidentified mixture, possibly because the strained four-membered ring is unstable in the presence of the NBS. Several other attempts were made to synthesize the dibromo four-membered ring silole compounds (Scheme 2). Compound **3** was treated with *n*-BuLi in THF and quenched with Me_3SnCl to afford an unidentified mixture of products. Tetrabromobithiophene was next lithiated with 2 equiv. of *n*-BuLi and quenched with Bu_3SnCl to give **6**.[62] Treating **6** with n-BuLi, followed by quenching with the appropriate cycloalkyl dichlorosilane afforded a complex mixture of products (Scheme 2). However, dibromo-functionalized monomers **7** and **8** could be prepared in 92−94% yield by bromination of **4** and **5**, respectively, using NBS in DMF (Scheme 3).

With the new dibromosilole building blocks in hand, annellated silole-based thiophene oligomers were synthesized via Stille coupling with the various trimethylstannyl thiophene reagents as shown Scheme 3. Compound **SM1**, obtained by reacting **8** with 5-hexyl-2-trimethylstannyl-thiophene, was isolated as a dark red oil in 80% yield. Similarly, reacting **8** with 5-trimethylstannyl-5′-hexyl-2, 2′-bithiophene affords **SM2** as a dark-red solid in 79% yield. The α,ω-unsubstituted oligomers **SM3** and **SM4** were also obtained by reaction of **7** and **8** with 2-trimethylstannyl bithiophene in 55−69% yield. For comparative purposes, dialkyl silole compound **SM5** was synthesized via reaction of known silole

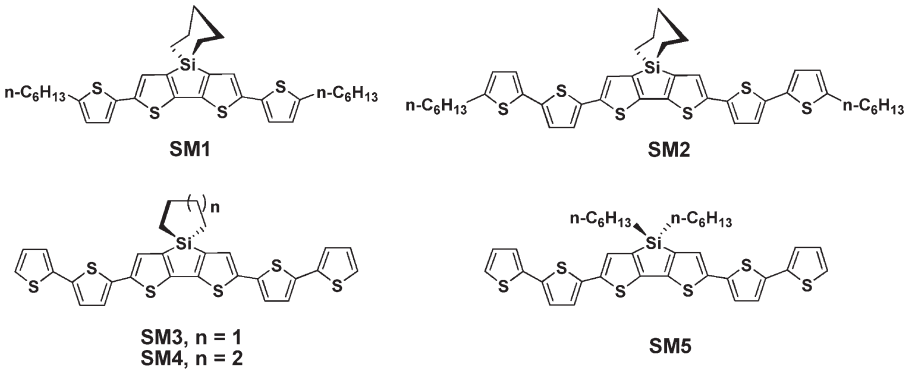

Figure 3. Structures of spiro-silole-based molecules **SM1**-**SM5**.

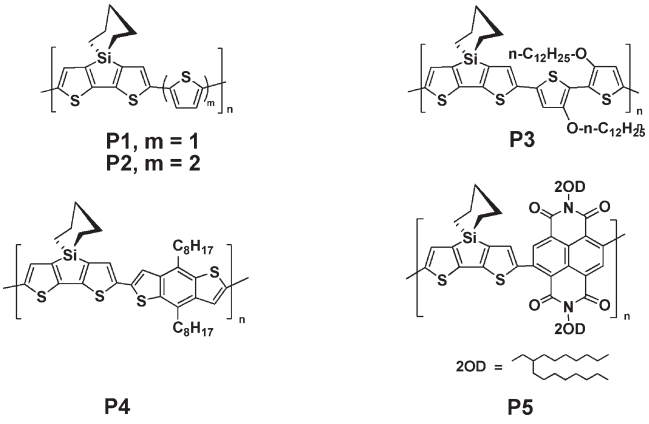

Figure 4. Structures of spiro-silole-based copolymers **P1**-**P5**.

Scheme 1. Synthesis of Spiro-dithienosiloles with Cycloalkyl Substituents

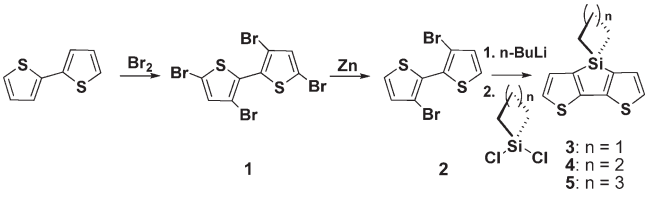

building block **9**[46] with 2-trimethylstannyl bithiophene, and was obtained as a dark-red solid in 85% yield.

Dithienosilole-based polymers **P1**−**P5** were synthesized via Stille polycondensation of **8** with 2,5-bis(trimethylstannyl)thiophene, 5,5′-bis(trimethylstannyl)-2,2′-bithiophene, 3,3′-dodecoxy-5,5′-bis(trimethylstannane)- 2,2′-bithiophene, 2,6-bis(trimethyltin)-4,8-dioctylbenzo[1,2-*b*:4,5-*b*′]dithiophene,[51] and *N*,*N*′-bis(2-octyldodecyl)- 1,4,5,8-naphthalenedicarboximide[52] in 52−87% yields as shown in Scheme 4. The physicochemical properties of these polymers are summarized in Table 1. Polymers **P1**, **P3**, **P5** are very soluble in common nonprotic organic solvents such as THF, toluene, xylenes, chloroform, chlorobenzene, and *o*-dichlorobenzene (DCB). The molecular weights (M_w) of polymers **P1**, **P3**, **P5** by GPC are 4.9 KD (PDI = 1.13), 32 KD (PDI = 6.0), 18 KD (PDI = 2.26), respectively. Polymers **P2** and **P4** are only soluble in hot chlorinated aromatic solvents such as chlorobenzene and DCB. Each of the new polymers was fully characterized by ^{1}H and ^{13}C NMR spectroscopy (broad features are observed as expected), optical spectroscopy, GPC, TGA, DSC, and elemental analysis. Details are given in the Experimental Section.

Silole Thermal Properties. The thermal properties of oligomers **SM2**−**SM5** and polymers **P1**−**P5** were investigated by thermogravimetric analysis (TGA), differential scanning calorimetry (DSC), and conventional melting point determinations. Figures 5 and 6 show representative TGA and DSC plots, and all data are collected in Table 1. Thermogravimetirc analysis (TGA, heating ramp rate = 10 °C/min under N_2) was used to investigate the thermal stability of the thiophene oligomers and polymers (Figure 5). In the thermolysis data, a 5% mass loss is defined as the thermolysis threshold. The thermolysis onset temperature for polymer **P1** is ∼250 °C, while oligomers **SM2**−**SM5** and all other polymers have onset temperatures above 300 °C, indicative of excellent thermal stability. This characteristic allows thin film annealing and microstructure analysis to be carried out over a broad range of temperatures, 50−300 °C. The observed melting points of compounds **SM3** and **SM4** are within 0−20 °C of the values observed by DSC (Table 1). We find that silicon substituent annellation has a substantial influence on oligomer thermal properties, doubtless reflecting an interplay of intermolecular $\pi-\pi$ stacking interactions and alkyl chain interdigitation. The melting point of the dialkyl compound **SM5** is 134−136 °C. Interestingly, this parameter increases to ∼240 °C for the annellated compounds **SM3** and **SM4**, indicating substantial differences in solid-state cohesive energies. Since the dipole moments of **SM3**-**SM5** are similar (vide infra), the significant increases in melting temperatures are likely the result of the less sterically demanding cyclic moieties of **SM3** and **SM4**, which thereby enhances intermolecular $\pi-\pi$ stacking. Interestingly, the melting points of **SM3** and **SM4** are independent of cycloalkyl ring size, which implies that similar intermolecular $\pi-\pi$ stacking energetics dominate. Note that the melting temperature of α,ω-di-*n*-hexyl substituted compound **SM2** is 144−146 °C. This indicates a significant reduction in the intermolecular cohesive forces, a phenomenon also observed in other conjugated organic semiconductors.[49,63]

The thermal properties of the present oligomers and polymers were also examined by differential scanning calorimetry (DSC) at a scanning speed of 10 °C/min (Figure 6). Oligomers **SM2** and **SM5** evidence no endotherms/exotherms in the heating/cooling cycles. Oligomer **SM3** exhibits a single endothermic peak at 238 °C, which is tentatively attributed to backbone melting,

Scheme 2. Synthetic Strategies to Prepare Spiro-cycloalkyl Silole Semiconductors Based on Compound 3

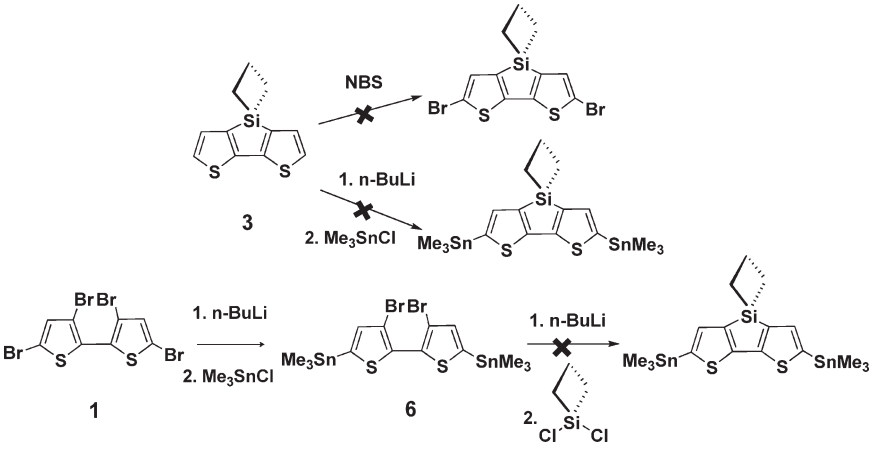

Scheme 3. Synthesis of Spiro-dithienosilole Monomers

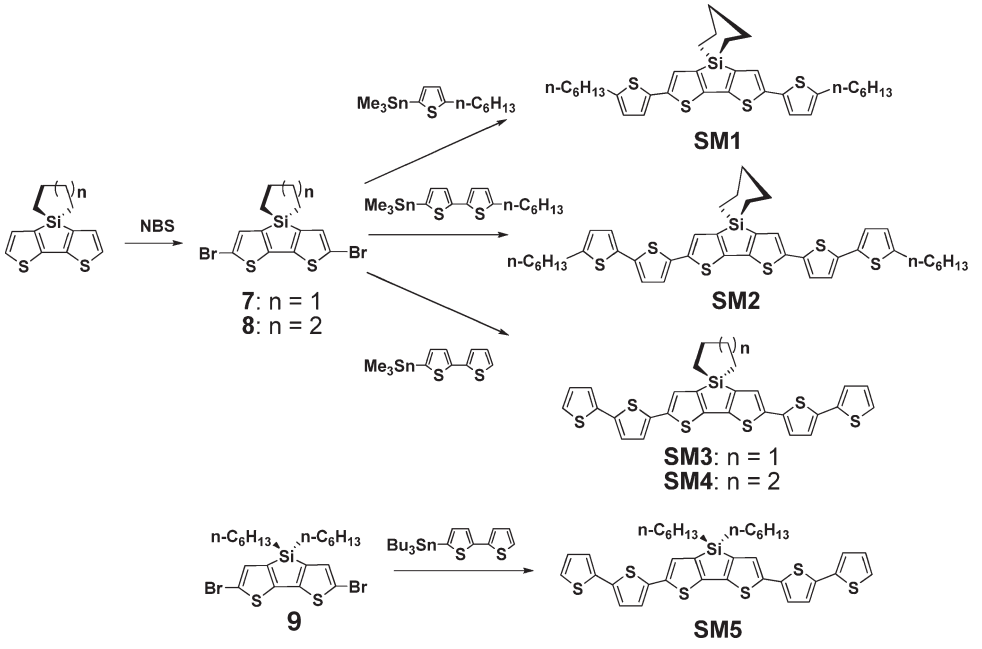

and an exothermic recrystallization peak upon cooling at 158 °C. Oligomer **SM4** exhibits a single endotherm at 246 °C, with a broad exotherm at 124 °C. Importantly, all four polymers have no endotherms/exotherms in the respective heating/cooling cycles, which implies that annealing of the semiconductors during the device fabrication will have little effect on OFET performance.

Silole Optical Properties. Solution and thin-film UV−vis absorption spectra of the present silole oligomers and polymers are shown in Figure 7, and data are collected in Table 1. Because of the presence of multiple absorption transitions and large Stokes shifts, solution and solid-state optical band gaps (E_g) were estimated from the low-energy band edges in the optical spectra.[64] The solution-based absorption and emission measurements were carried out at very low concentrations ($<10^{-5}$ M) in a solvent of intermediate dielectric constant (DCB, ε = 9.8) to minimize the influence of molecular aggregation and differences in molecular dipole moments (solvents with large dielectric constants can preferentially stabilize polar molecular conformations), and thereby revealing the "intrinsic" molecular structural features such as planarity, optical HOMO−LUMO gap, and extent of π-conjugation.[65]

Compounds **SM3** and **SM4** have similar optical absorption spectra and exhibit essentially the same optical absorption maxima at 473 nm. The corresponding spin-coated thin films exhibit absorption maxima at 487 nm (with a strong shoulder at 524 nm) and 484 nm (with a strong shoulder at 522 nm), respectively. Compound **SM2** has an optical absorption maximum at 482 nm in DCB solution and at 491 nm for thin films. Both of the **SM2** maxima are at slightly larger energies than those of **SM4**, reflecting the electron-donating properties of the terminal *n*-hexyl chains. All of the absorption maxima for oligomers **SM2**-**SM4** exhibit small red-shifts

dx.doi.org/10.1021/cm200009k |*Chem. Mater.* 2011, 23, 2185–2200

Scheme 4. Synthesis of Annellated Spiro-dithienosilole-based Copolymers

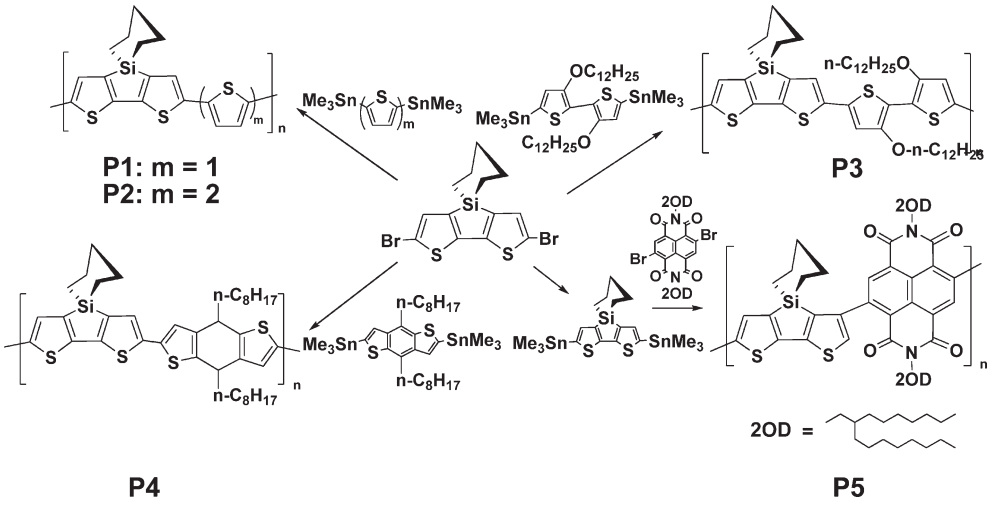

Table 1. Summary of Thermal, Optical Absorption/Emission, and Electrochemical Properties of Silole Compounds SM2-SM5, P1−P5, and the Corresponding Estimated Frontier Molecular Orbital Energies

compd	mp (°C)	T_{DSC} (°C)[a] heating (cooling)	T_{TGA} (°C)[b]	$E^{red\text{-}1/2}$ (V)[c]	$E^{ox\text{-}1}$ (V)[c]	E_g^{CV} (eV)[c]	E_{LUMO} (eV)[d]	E_{HOMO} (eV)[e]	$\lambda_{abs}^{solution}$ (nm)[f]	$\lambda_{abs}^{thin\text{-}film}$ (nm) (E_g(eV))[g]	λ_{em}^{sol} (nm)[h]
SM2	144−146	NA	413	−1.4	1.0	2.4	−3.4	−5.4	482	491 (2.0)	521
SM3	236−238	258 (158)	350	−1.2	1.1	2.3	−3.4	−5.5	473	487,524 (2.1)	520
SM4	244−246	246, 124	303	−1.3	1.1	2.4	−3.4	−5.5	473	484, 522 (2.1)	537
SM5	134−136	NA	320	−1.2	1.2	2.4	−3.5	−5.6	466	447 (2.1)	603
P1		NA	250	−1.0	1.0	2.0	−3.5	−5.4	508	532 (1.9)	612
P2		NA	320	−0.9	1.1	2.0	−3.6	−5.5	542	560 (1.9)	623
P3		NA	320	−1.2	0.7	1.9	−3.4	−5.1	586	608 (1.7)	688
P4		NA	415	−1.1	0.8	1.9	−3.3	−5.2	548	542 (1.9)	657
P5		NA	412	−0.4	1.2	1.6	−4.0	−5.6	392, 681	400, 755 (1.4)	439, 539 (392)[i] 793, 913 (681)[i]

[a] From DSC scans under nitrogen at a scan rate of 10 °C/min. [b] Onset decomposition temperature measured by thermogravimetric analysis under nitrogen. [c] For oligomers, 0.1 M $Bu_4N^+PF_6^-$ in THF (vs SCE) at a scan rate of 100 mV/s. For polymers, as thin films with 0.1 M $Bu_4N^+PF_6^-$ in acetonitrile (vs SCE). [d] E_{LUMO} is calculated from: $E_g = E_{LUMO} - E_{HOMO}$. [e] Estimated from the equation: $E_{HUMO} = -4.4$ eV $- E_{sol.}^{red\text{-}1/2}$. [f] From optical absorption in DCB. [g] From optical absorption as spin-coated thin-film on glass, optical band gap is estimated from the low energy band edge of the UV−vis spectrum. [h] From optical emission in DCB. [i] Broad, weak emission peak.

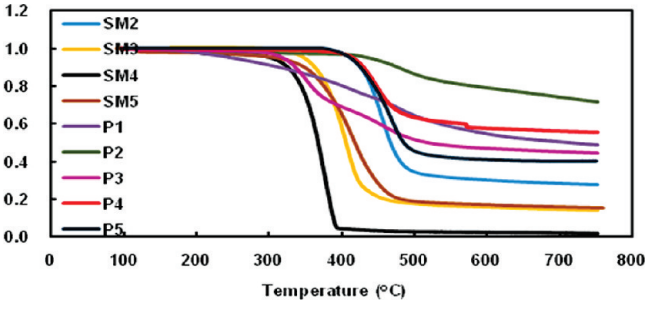

Figure 5. Thermogravimetric analysis (TGA) of oligomers and polymers at a temperature ramp of 10 °C/min under N_2.

upon going from the solution to thin film phase, indicating on average a somewhat greater degree of organization in the thin film phase. Note, however, that the optical absorption spectrum of **SM5** has a maximum at 466 nm in DCB solution, but a maximum at 447 nm in thin films on glass. This hypsochromatic shift of the dominant absorption band suggests that H-aggregate formation may occur in the solid state,[66] in which the molecules are cofacially aligned.

To better understand the electronic spectra of the present silole molecules, time-dependent density functional theory (DFT) calculations (TD-DFT) were performed, and the 12 frontier MO energies estimated. Selected data are shown in Table 2. These calculations predict that the electronic transitions having the highest oscillator strengths are located at 535, 533, and 532 nm for **SM3**, **SM4**, and **SM5** respectively, and correspond to monoelectronic excitation from the highest occupied molecular orbital (HOMO) to the lowest unoccupied molecular orbital (LUMO). The differences found between theoretical and experimental wavelengths can be ascribed both to the fact that the calculations are carried out considering isolated molecules in vacuo vs the solution phase or solid-state in which experimental data are acquired, and to the tendency of DFT to overestimate π-conjugation.[67] Figure 8 shows the topologies of the frontier molecular orbitals involved in the

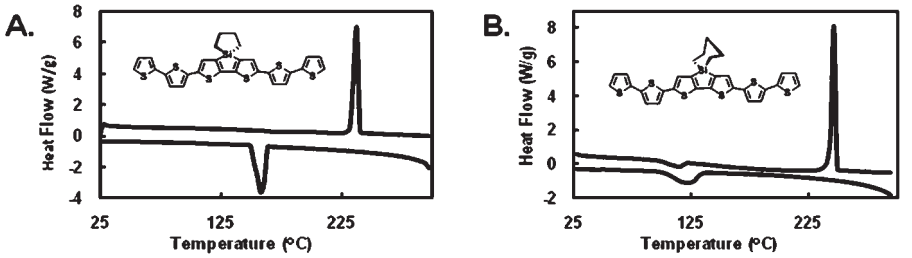

Figure 6. Differential scanning calorimetry (DSC) of the spiro-silole oligomers (A) **SM3** and (B) **SM4** at a temperature ramp of 10 °C/min under N_2.

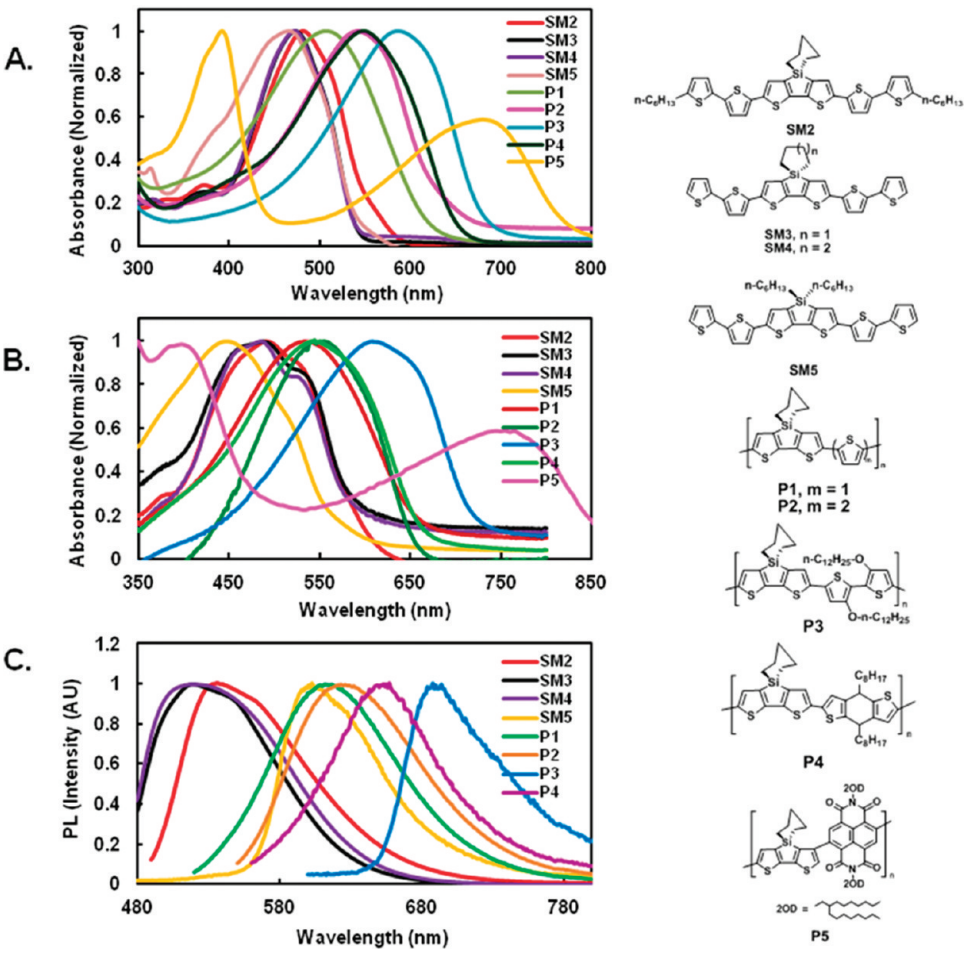

Figure 7. Optical absorption spectra of annellated silole oligomers and polymers (A) in DCB solution and (B) as thin films on glass substrates, and (C) photoluminescence spectra in DCB solution.

highest oscillator strength electronic transition for molecules **SM3**, **SM4**, and **SM5**. As also found in oligothiophenes, the HOMOs are aromatic in nature, with no significant contributions of the S or Si orbitals, and are basically linear combinations of the fused core HOMOs with the thiophene HOMOs. This result suggests that Si inclusion in the oligothiophene backbone should not significantly affect oxidation potentials, in agreement with the present (see below) and previous results on related systems.[46] Nevertheless, it is interesting to note that the greatest contribution to the HOMO comes from the central fused silole moiety and the nearby thiophene rings, with lesser contributions from the external thiophene rings. In the case of the LUMOs, the topologies for the three compounds have a distinctive quinoidal character, with a significant contribution from the S atoms, while the contribution of the Si atoms remains negligible.[46] As expected, the substitution of linear or branched alkyl chains by cycloalkyl ones does not induce any significant changes in either the energies or molecular topologies of the frontier orbitals, making it clear that any variations in TFT electrical performance should be solely ascribed to changes in crystal packing and/or microstructure effects rather than to differences in molecular electronic structure.

As noted above and summarized in Table 1, the optical absorption spectra of the annellated silole polymers exhibit absorption maxima that are red-shifted versus those of the corresponding oligomers, suggesting extended π-conjugation. The absorption maxima of **P1**, **P2**, **P3** and **P4** in solution are located at 508 nm, 542 nm, 586 nm, and 548 nm, respectively,

dx.doi.org/10.1021/cm200009k |*Chem. Mater.* 2011, 23, 2185–2200

Table 2. Summary of Computed (DFT//B3LYP/6-31G) Frontier Molecular Orbital Energies, HOMO-LUMO Gaps, Highest Oscillator Strength Transition Energies, Oscillator Strengths, and Excited-State Configurations as Determined by TDDFT Calculations. Theoretical (DFT//B3LYP/6-31G**) Reorganization Energies for Hole Injection for Molecules SM3, SM4, and SM5**

compd	HOMO (eV)	LUMO (eV)	$E_{g,theor.}$(eV)	λ (nm)	osc. str.	configuration	λ (eV)
SM3	−4.71	−2.14	2.57	535	1.70	HOMO→LUMO	0.308
				324	0.33	H-2→L	
						H-1→L+1	
						H→L+4	
SM4	−4.70	−2.13	2.57	533	1.74	HOMO→LUMO	0.318
				323	0.31	H-2→L	
						H-1→L+1	
						H→L+4	
SM5	−4.68	−2.11	2.57	532	1.74	HOMO→LUMO	0.321
				322	0.29	H-2→L	
						H-1→L+1	
						H→L+2	
						H→L+4	

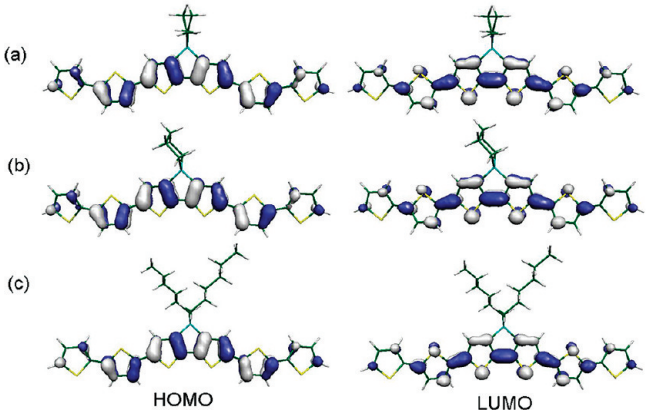

Figure 8. B3LYP/6-31G** electronic density contours for the frontier molecular orbitals of: (a) **SM3**, (b) **SM4**, and (c) **SM5**.

while those of the corresponding thin films are located at 532 nm for **P1**, 560 nm for **P2**, 608 nm for **P3**, and 542 nm for **P4**. The absorption maxima of **P5** occur at 680 and 392 nm in DCB solution and at 755 and 400 nm for the thin film, corresponding to the smallest $\pi-\pi^*$ transition energy in the silole-based polymer series and indicating that the strongest electron-accepting NDI building block affords the lowest LUMO energy and leads to the smallest HOMO−LUMO gap.

The optical band gaps for the oligomers and polymers were estimated from the low-energy band edges of the thin-film optical spectra, taking 10% of the maximum as the band edge. The optical band gaps of oligomers **SM2**, **SM3**, **SM4**, and **SM5** are 2.08, 2.08, 2.05, and 2.07 eV, respectively, significantly smaller than that of α-6T (2.30 eV).[68] However, the optical band gaps of polymers **P1**, **P2**, **P4** are 1.89, 1.90, and 1.87 eV, respectively, similar to that of P3HT (1.9 eV),[69] and to those of **TS6T1** and **TS6T2** (1.8−1.9 eV; Figure 1).[44,46] These small band gaps likely reflect the appreciable planarity of these macromolecules (vide infra) and a backbone similarity to that of polythiophenes. Note that polymer **P3** has a particularly small optical band gap of 1.72 eV, indicating that the oxyalkyl subsituent is a strongly electron-donating group, resulting in a higher-lying HOMO. Also, the smallest band gap of **P5** (1.4 eV) is comparable to those reported for NDI-based copolymers.[52,70]

The silole solution PL emission spectra are shown in Figure 7C and data are collected in Table 1. Because 0−0 transitions are rarely observed in room temperature solution spectra, it is an accepted procedure to use $\Delta = \lambda_{em} - \lambda_{abs}$ as an estimation of the magnitude of the Stokes shift.[71] The silole-based oligomers **SM2**, **SM3**, and **SM4** emit green-yellow light with maxima at 521, 520, and 537 nm, respectively, while **SM5** emits orange-red light with maximum at 603 nm. These transitions are assigned to the 0−1 transition in dilute solutions. The silole-based oligomer **SM5** exhibits much larger Stokes' shifts (137 nm) than **SM4** (64 nm), suggesting that the long alkyl chains on the tetrahedral Si provide greater degrees of molecular freedom than do the constrained cycloalkyl substituents (more rotational/vibrational states from which to dissipate energy). Such large Stokes' shifts are also observed in fluorene systems having long alkyl chains at the bridgehead carbon atom of the backbone.[72] Molecule **SM2** with pedant alkyl chains in the backbone exhibits a smaller Stokes' shift (39 nm) than does **SM4** (64 nm). Similar trends are also observed for the polythiophenes functionalized with pedant alkyl chains, where longer chains afford smaller Stokes' shifts,[73] suggesting that the **SM2** backbone is more rigid.[74,75] Similarly, the Stokes' shift of **SM3** (47 nm) is slightly smaller than that of **SM4** (64 nm), indicative of the greater **SM3** backbone rigidity.

Silole-based polymers **P1** and **P2** emit orange light with emission maxima located at 612 and 623 nm, while **P3** and **P4** emit red light with emission maxima located at 688 and 657 nm. All of these polymers exhibit large Stokes' shifts of ∼80−110 nm, which are not unusual for silicon-containing polymers,[46,76] and may possibly be due to eximer emission.[77,78] However, when electron-deficient polymer **P5** is excited at the short-wavelength (392 nm) or at the long-wavelength absorption maximum (681 nm), only very weak, broad emissions having shapes similar to the absorption spectra are observed with maxima at 439, 539 nm or 793, 913 nm, respectively. This is consistent with the general observation that increased Stokes shift amplitudes generally correlate with longer excited-state lifetimes, resulting in an increase in the relative probability of nonradiative decay and lower PL quantum efficiencies.[79] This suggests for the present

dx.doi.org/10.1021/cm200009k |*Chem. Mater.* 2011, 23, 2185–2200

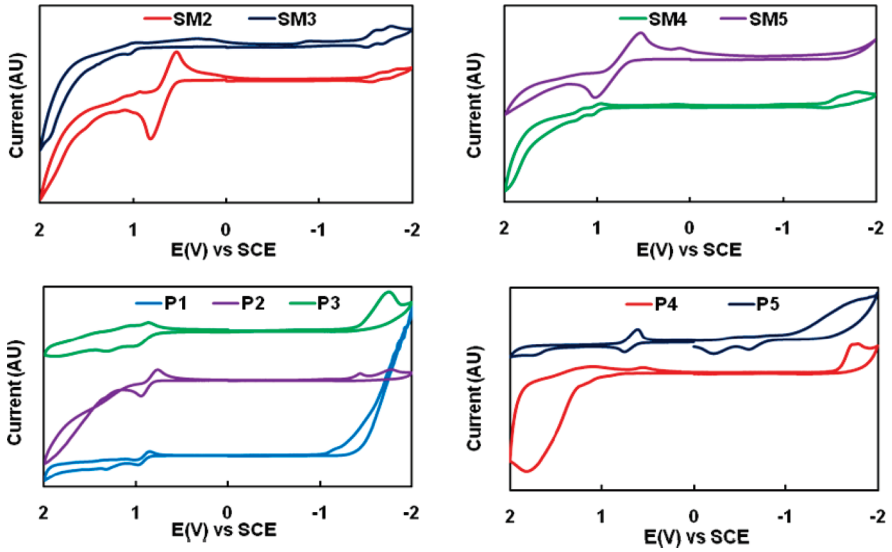

Figure 9. Cyclic voltammograms of molecules **SM2-SM5** as solution in THF with 0.1 M $Bu_4N^+PF_6^-$ suppoting electrolyte and polymers **P1**−**P5** as thin films in acetonitrile with 0.1 M $Bu_4N^+PF_6^-$ supporting electrolyte at scan rates of 100 mV/s.

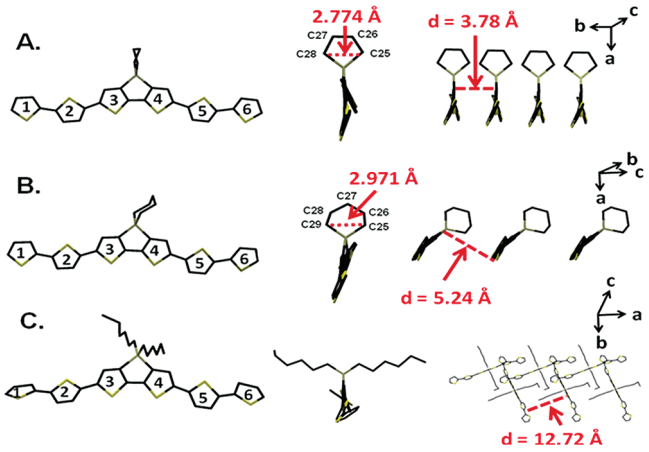

Figure 10. Diffraction-derived single-crystal structures of (A) **SM3**, (B) **SM4**, and (C) **SM5**. Hydrogen atoms are omitted for clarity. The distance indicated by *d* is the shortest interplanar $\pi-\pi$ contact.

siloles that the core electron-deficiency facilitates intramolecular charge-transfers which result in large Stokes shifts and eventual quenching.[80]

Silole Electrochemical Properties. Oxidation and reduction potentials for the present oligomers and polymers were measured by cyclic voltammetry (CV) experiments. Cyclic voltammograms of the oligomers in THF and the polymers as thin films are shown in Figure 9, and electrochemical data are summarized in Table 1. The ferrocene/ferrocenium couple was used as the internal standard. The silole-based oligomers **SM2**, **SM3**, **SM4**, and **SM5** exhibit reduction/oxidation potential onsets at −1.4/1.0, −1.2/1.1, −1.3/1.1, and −1.2/1.2 V, respectively (vs SCE). The onset potentials for the polymers are at −1.0/1.0, −0.9/1.1, −1.2/0.7, −1.1/0.8, and −0.4/1.2 V (vs SCE) for **P1**, **P2**, **P3**, **P4**, and **P5**, respectively. The smallest onset oxidative potentials of **P3** suggest a lower stability with respect to oxidative doping.

From the oxidation potentials, the ionization potentials ($IP^{ox} \approx -HOMO^{ox}$, assuming that Koopmans' theorem holds) for the present oligomers and polymers can be estimated by taking the SCE energy level to be −4.4 eV below the vacuum level and using the standard relationship of eqs 1 and 2.[81]

$$HOMO^{ox} = -E_{ox\text{-}onset} - 4.4 \quad (1)$$

$$E_g = E_{LUMO} - E_{HOMO} \quad (2)$$

Using relationships (1) and (2), the HOMO/LUMO energies are estimated as −5.4/-3.4 eV for **SM2**, −5.5/-3.4 eV for **SM3**, −5.5/-3.4 eV for **SM4**, −5.6/−3.5 for **SM5**. Similarly, polymers **P1**, **P2**, **P3**, **P4**, and **P5** have HOMO/LUMO energies at −5.4/-3.5 eV, −5.5/−3.6 eV, −5.1/−3.4 eV, −5.2/−3.3 eV, −5.6/−4.0 eV. respectively, indicative of significantly greater ionization energies than P3HT (∼4.9 eV).[82] Clearly, introduction of the silole core into the thiophene backbone stabilizes the system with respect to ionization without sacrificing π-conjugation, as argued by the similar optical band gaps (vide supra). The HOMO/LUMO energies of the present polymers with cycloalkyl substituents are comparable to those of the silole-based polymers having long alkyl chain substituents.[44,46]

As shown in Table 2, DFT calculations estimate the HOMO and LUMO energies to be −4.71/−2.14 eV, −4.70/−2.13, and −4.68/−2.11 eV for compounds **SM3**, **SM4**, and **SM5**, respectively, leading to a uniform HOMO−LUMO energy gap of 2.57 eV. This value is in good agreement with the experimental band gaps obtained from the electrochemical results (Table 1), which range from 2.3 to 2.4 eV.

Single-Crystal Molecular Structures. Single crystals of the new silole compounds **SM3**, **SM4**, and **SM5** were grown by slow diffusion of hexane or methanol into DCB solutions, and the crystal structures are shown in Figure 10. The introduction of the silole functional group into the sexithiophene backbone causes twisting of the **SM3**, **SM4**, and **SM5** backbones from planarity, and the change in Si substituents from linear long alkyl chains to cycloalkyls results in major changes in the solid state packing. For molecule **SM3**, the twist angles between rings 2 and 3, and between rings 4 and 5 are 20.17 and 11.80°, respectively, which is much larger than those observed in sexithiophene (∼3−4°)[83]

dx.doi.org/10.1021/cm200009k |*Chem. Mater.* 2011, 23, 2185–2200

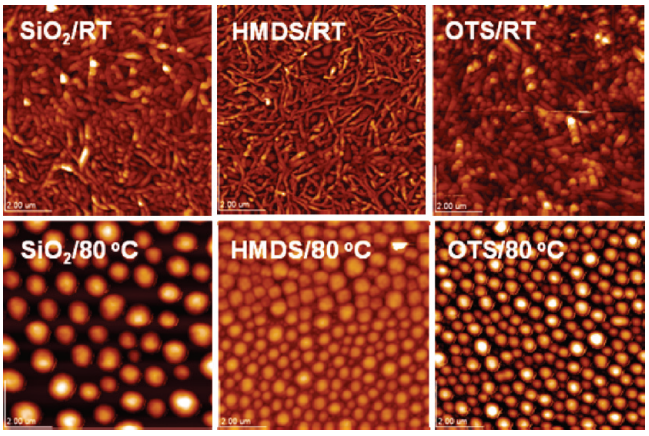

Figure 11. Tapping-mode AFM images of **SM3** thin films grown at the indicated temperatures and on various substrates (scan areas: 9 μm × 9 μm).

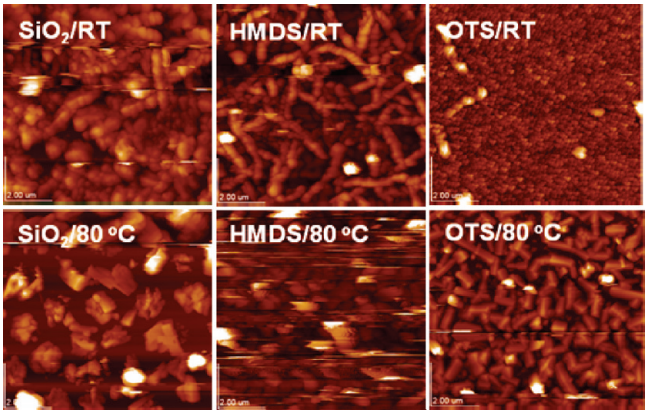

Figure 12. Tapping-mode AFM images of **SM4** thin films grown at the indicated temperatures and on various substrates (scan areas: 9 μm × 9 μm).

and in alkyl-subsituted oligothiophenes (~5−6°).[20,84] The **SM3** twist angle values are midway between a planar configuration and ~30°, the latter being the maximum value beyond which there is insufficient intramolecular π-overlap to achieve a significantly π-conjugated structure.[85] The twist angles between **SM3** rings 1 and 2, 3 and 4, and 5 and 6, are much smaller, 1.53, 5.50, and 4.68°, respectively. The exocyclic silacyclopentane ring is twisted and the distance between atoms C25 and C28 is 2.774 Å, while the theoretical distance from DFT calculations is 2.822 Å. The twisted confomation of the silacyclopentane is similar to that of other reported silacylopentanes.[61,86,87] In regard to packing, the conjugated backbones of the **SM3** molecules are partially π−π stacked in a slipped cofacial orientation along the *b* axis. The minimum π−π distance between the closest thiophene rings is ~3.78 Å. For compound **SM4**, the thiophene-thiophene twist angles are 7.2, 21.2, 4.64, 13.0, and 10.8° on proceeding from ring 1 to 6, respectively. The highly twisted structure suggests unoptimized intramolecular conjugation, probably hindering charge transporting efficiency. The silacyclohexane ring adopts a chair conformation with a distance between C25 and C29 of 2.971 Å, while the theoretical distance from the DFT calculation is 2.993 Å. Such a chair confomation of the silacyclohexane substituent has been observed in related molecules.[86−88] As can

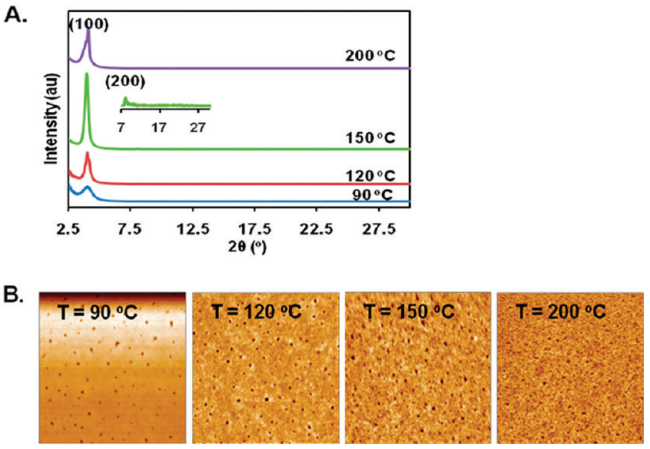

Figure 13. (A) θ−2θ X-ray diffraction (XRD) scans of spin-coated **P5** thin films after annealing at the indicated temperatures. Note that peak intensities are not normalized). (B) Tapping mode AFM images of **P5** thin films after annealing at the indicated temperatures on different substrates (scan areas: 4.5 μm × 4.5 μm).

be seen in Figure 10, the backbones of successive **SM4** molecules assemble in a slipped herringbone conformation along the *a* axis with a minimum cofacial distance between the closest thiophene rings of 5.24 Å, which is significantly larger than that in **SM3**. For compound **SM5** having two Si-*n*-hexyl chains, the backbone is significantly twisted with thiophene-thiophene twist angles of 31.7, 25.3, 2.8, 21.8, and 27.3° on going from ring 1 to 6, respectively, indicating weak intramolecular π conjugation. Futhermore, the molecular backbones stack along the *a* axis in a slipped herringbone motif having a large minimum distance between the neighboring backbones of 12.72 Å, indicating negligible π−π stacking interactions. The long *n*-hexyl chains occupy/create the large free volume between adjacent molecules. Thus, through cyclization of the silicon alkyl substitents, it can be seen that closer distances between the neighboring π backbones are achieved (**SM3** < **SM4** < **SM5**), representing a heretofore unexplored strategy for enhancing π−π stacking. This is consistent with the change of the calculated density according to the crystal data, **SM3** (1.526 g/mm^3) > **SM4** (1.477 g/mm^3) > **SM5** (1.301 g/mm^3). Furthermore, it will be seen that these crystal structure observations are consistent with the charge transporting properties of the TFT devices fabricated with these oligomers (vide infra).

Thin-Film Microstructure and Morphology. Thin film microstructure, morphology, and molecular orientations for the present new class of materials were studied by θ−2θ X-ray diffraction (XRD) and atomic force microscopy (AFM). Measurements were carried out on vacuum-deposited and spin-coated thin films grown on OTS-treated Si/SiO_2 substrates. The thicknesses of all films were 50−60 nm as measured by profilometry. The XRD scans reveal that the films of all the oligomers as well as polymers **P1**-**P4** are essentially amorphous, even films of the polymers annealed overnight at 250 °C. AFM images of the vacuum-deposited films of the oligomers indicate that the morphologies of the films depend on the substrate surface energy and the deposition temperature as shown in Figures 11 and 12.

The morphology of the vacuum-deposited **SM3** films consists of rounded grains on bare SiO_2 and OTS-treated substrates when grown at room temperature, however worm-like grains are

Table 3. Field-Effect Mobilities (μ_h), Threshold Voltages (V_T), and Current I_{on}/I_{off} Ratios for Thin Films of Silole Compounds SM3, SM4, and P1−P5 Fabricated by Vacuum-Deposition/Spin Coating on Bare SiO_2, HMDS-Treated, and OTS-Treated Si/p^+-SiO_2 Substrates

	SM3[a]		SM4[a]			P1[b]	P2[b]		P3[b]		P4[b]		P5[b]		
	OTS[c]	OTS[d]	SiO_2[c]	HMDS[c]	OTS[c]	190 °C[e]	110 °C[e]	190 °C[e]	110 °C[e]	190 °C[e]	110 °C[e]	190 °C[e]	90 °C[e]	150 °C[e]	200 °C[e]
μ ($cm^2/(V\,s)$)	9.3×10^{-6}	4×10^{-4}	8.0×10^{-5}	1.0×10^{-4}	3×10^{-4}	2.4×10^{-5}	6×10^{-4}	6×10^{-4}	3×10^{-4}	3×10^{-4}	1×10^{-3}	2×10^{-3}	1×10^{-3}	4×10^{-3}	2×10^{-3}
I_{on}/I_{off}	3×10^2	2×10^3	2×10^4	5×10^3	1×10^5	1×10^3	1×10^2	1×10^5	0	10	1×10^2	1×10^2	1×10^2	1×10^2	1×10^2
V_T (V)	−22	−8	−8	−15	−13	−5	14	17	−34 to 17	−34 to 17	17	−3 to 15	15	17	15

[a] Fabricated by vacuum-deposition. [b] Fabricated by spin-coating. [c] Deposition temperature of substrate T_d = 20 °C;. [d] Deposition temperature of substrate T_d = 80 °C. [e] Annealed at the indicated temperature for 2 h.

observed on HMDS-treated substrates. For growth at 80 °C, significant plate-shaped grains with sizes of >1 μm are observed, but also large grain boundaries are found on bare SiO_2, portending poor charge transport efficiency. Nevertheless, the film morphologies having large worm-like grains on OTS-treated substrates may be favorable for charge transport. In room temperature depositions, the morphology of the vacuum-deposited **SM4** films changes from rounded grains with dimensions <0.1 μm on bare SiO_2 to dimensions >0.2 μm on OTS-treated substrates, while the morphology of the films has worm-like grains on HMDS-treated substrates. When films of the same compound are vacuum-deposited at 80 °C, the film morphology is characterized by grains with very large intervening boundaries.

In marked contrast to the above results, XRD scans reveal that **P5** films are crystalline as shown in Figure 13. A single family of diffraction peaks is observed without the presence of an obvious $\pi-\pi$ stacking distance, and the *d*-spacing is estimated from the (100) reflection to be 21.6 Å (after 200 °C annealing), implicating a crystalline polymorph where the majority of the molecules have an edge-on orientation on the substrate with the $\pi-\pi$ stacking direction parallel to the substrate plane, thereby favoring in-plane charge transport from source to drain. The degrees of crystallinity of the solution-cast **P5** films are dependent on the annealing temperature. As shown in Figure 13, a possible change in the preferential crystalline phase/orientation is observed upon annealing, with the *d*-spacing decreasing from 23.6 to 21.9 Å from 90 to 150 °C, with a significant increase in the (100) reflection intensity (13,000 to 65,000 counts/s), and with the appearance of a higher order reflection (200), indicative of a higher degree of ordering, and presumably increased alkyl-chain interdigitation. Note however that annealing at even higher temperature (200 °C) decreases the reflection intensity (65 000 to 36 000 counts/s) and diminishes the higher order reflections, whereas the *d*-spacing continuously decreases to 21.6 Å. AFM analysis shows the upon annealing, the film morphology changes, but not in major ways. At 150 °C, the grain sizes appear to have the maximum dimensions vs the other annealing temperatures. Note that these morphological results are consistent with the transistor performance (vide infra).

Thin-Film Transistor Characterization. Top-contact/bottom-gate OTFTs devices were fabricated on bare SiO_2 as well as on HMDS-, and OTS-treated SiO_2/p^+-Si substrates. All oligomer films were vapor-deposited under high vacuum (1×10^{-6} Torr) with the substrates maintained at temperatures of 21 or 80 °C. Finally, Au source and drain contacts were deposited by thermal evaporation using a shadow mask to define channel lengths (L) of 25−100 μm and widths (W) of 500−2000 μm. Bottom-contact/top-gate polymer OTFTs were fabricated by spin-coating with 7 mg/mL polymer in DCB solutions. In this case, the spin-coating processes were carried out in air on glass substrates having thermally deposited Au source and drain electrodes with a W/L ratio of 10. The thin polymer films were next annealed under vacuum and a PMMA gate dielectric spin-coated on top of the semiconductor film, and the assembly dried in a vacuum oven. Next, gold gate electrodes were deposited by thermal evaporation. FET properties were then evaluated under positive or negative gate bias in ambient and vacuum to define the majority charge carrier type, device performance, and environmental stability. The field-effect mobility and threshold voltages are calculated in the saturation regime. FET data are summarized in Table 3, and representative transfer plots are shown in Figure 14.

Devices fabricated with oligomers **SM2** and **SM5** are found to be FET-inactive, whereas compounds **SM3** and **SM4** are

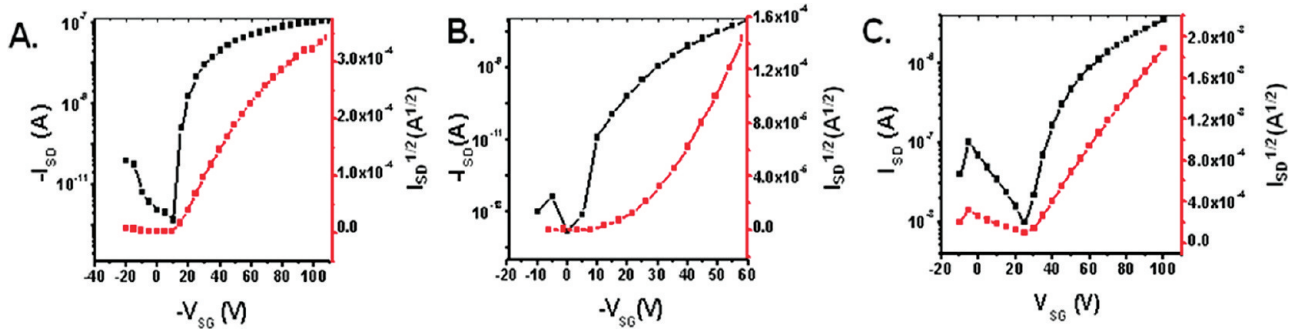

Figure 14. OTFT transfer plots of polymers (A) **SM4**, (B) **P2**, (C) **P5** at $V_{SD} = -100$ V.

Table 4. Summary of Crystallographic Data for SM3, SM4, and SM5

	SM3	SM4	SM5
formula	$C_{28}H_{20}S_6Si$	$C_{29}H_{22}S_6Si$	$C_{36}H_{38}S_6Si$
fw	576.89	590.92	691.11
space group	$P2(1)/n$	$Pna2(1)$	$P\bar{1}$
a (Å)	20.858(2)	11.1140(5)	13.681(3)
b (Å)	5.0475(6)	32.1250(14)	13.705(3)
c (Å)	25.530(3)	7.4428(4)	19.382(4)
α (deg)	90	90	100.457(13)
β (deg)	110.948(7)	90	98.896(13)
γ (deg)	90	90	89.817(13)
V (Å^3)	2510.2(5)	2657.4(2)	3529.7(12)
Z	4	4	4
D (calcd), g cm^{-3}	1.526	1.477	1.301
μ (mm^{-1})	5.628	5.330	0.446
T (K)	100(2)	100(2)	100(2)
diffractometer	Bruker Apex2 CCD	Bruker Apex2 CCD	Bruker Apex2 CCD
radiation	CuKα (1.5418 Å)	CuKα (1.5418 Å)	MoKα (0.71073 Å)
cryst size (mm^3)	0.19 × 0.08 × 0.04	0.47 × 0.15 × 0.05	0.32x 0.21x 0.11
F(000)	1192	1224	1456
measd reflns	2186	10048	13029
independent reflns	2350	2855	6672
$R(F)$ (%)[a]	0.0666	0.0450	0.2432
R (wF^2) (%)[b]	0.1091	0.0459	0.4306

[a] $R = \Sigma||F_o| - |F_c||/\Sigma|F_o|$. [b] $R(\omega F^2) = \{\Sigma[\omega(F_o^2 - F_c^2)^2]/\Sigma[\omega(F_o^2)^2]\}^{1/2}$; $\omega = 1/[\sigma^2(F_o^2) + (aP)^2 + bP]$, $P = [2F_c^2 + \max(F_o,0)]/3$.

p-channel semiconductors. It is not surprising that compound **SM5** is an inactive charge-transporting material since the long Si-alkyl chains prevent close $\pi-\pi$ stacking of the cores as discussed above. In contrast, the **SM4** silacyclohexane structure allows close $\pi-\pi$ stacking, and the charge transport is significantly enhanced with TFTs exhibiting mobilities of ~3 × 10^{-4} cm^2/(V s) and I_{on}/I_{off} ratios of ~1 × 10^5 on OTS-treated substrates. Note that all films deposited at 80 °C are FET-inactive, in agreement with the AFM morphology results discussed above. The introduction of α,ω-hexyl substituents in molecule **SM2** is detrimental to the charge transport capacity and negligible performance is observed in FETs. After reducing the size of the silacycloalkyl substituents from 6- to 5-membered rings, **SM3**−based FETs exhibit enhanced performance with hole mobilities of ~4 × 10^{-4} cm^2/V·s and I_{on}/I_{off} ratios of 2 × 10^3 on OTS-treated substrates. It is not surprising that the FET performance of oligomers **SM3** and **SM4** is below that of sexithiophene (μ = 0.02 cm^2/V·s),[89] not only because of the bulky cycloalkyl chains, but also because of the twisted conformations of the **SM3** and **SM4** backbones. However, the mobilities of **SM3** and **SM4** are superior to those reported for dithienosilole oligomers **sDTS-1** and **DTS-3T** (1 × 10^{-7} to 1 × 10^{-5} cm^2/(V s))[43,] (Figure 1). All of the present devices show similar mobilities when measured in vacuum or under ambient conditions, indicative of good environmental stability, and consistent with the low-lying HOMOs (−5.4 to −5.6 eV) of these oligomers.

The four polymers **P1**−**P4** are found to be p-channel semiconductors, while **P5** is an n-channel semiconductor. Thermal annealing is found to marginally improve the TFT response of the devices fabricated with polymers **P1**−**P4**, consistent with the XRD results discussed above, which reveal minimal crystallinity. Bottom-contact/top-gate TFTs fabricated with polymer **P1** exhibit a hole mobility of 4 × 10^{-5} cm^2/(V s) and an I_{on}/I_{off} ratio ~1 × 10^3. Devices fabricated with the more π-extended polymer **P2** show improved performance with μ ~ 6 × 10^{-4} cm^2/(V s) and I_{on}/I_{off} ratio ~1 × 10^5. This trend was also observed in silole polymers **TS6T1** and **TS6T2** (Figure 1).[44,46] However, the solubility of polymer **P2** is poor due to lack of long alkyl substituents. Thus, long alkoxyl chains were introduced in polymer **P3** to enhance the solubility. However, note that the TFT performance of **P3** is similar to that of polymer **P2** with a mobility of 3 × 10^{-4} cm^2/(V s) and an I_{on}/I_{off} ratio ≈ 10. This is perhaps not surprising because the **P3** films are amorphous, even after high temperature annealing. In contrast, polymer **P4** containing a more rigid building block in the backbone exhibits superior TFT performance with a mobility of ~0.001 cm^2/(V s) and I_{on}/I_{off} ≈ 1 × 10^2 after annealing at 110 °C for 2 h, and ~0.002 cm^2/V·s and I_{on}/I_{off} ≈ 10^2−10^3 after annealing at higher temperatures (190 °C, 2 h). Comparing the device performance of these p-channel polymers, the general trends are that the mobility increases as more thiophene rings are introduced into the backbone (polymers **P1** and **P2**) and when a more rigid building block is used (polymers **P3** and **P4**). Nevertheless, the amorphous morphology of these polymer films leads to modest TFT device performance. Top contact/bottom gate TFTs fabricated with polymer **P5** exhibit an electron mobility of 0.0001 cm^2/(V s) and an I_{on}/I_{off} ratio ~1 × 10^2 after annealing at 120 °C for 2 h. The mobility increases to 0.004 cm^2/(V s) after annealing the film at 150 °C for 2 h.

However, thermal annealing at higher temperature (200 °C, 2 h) decreases the mobility (0.002 $cm^2/(V\,s)$). Importantly, the device performance is consistent with the microstructures and morphologies as deduced by XRD and AFM as discussed above.

CONCLUSIONS

A new series of silole-containing oligomers **SM2**−**SM5** and copolymers **P1**−**P5** with silacycloalkyl substituents has been synthesized and characterized by DSC, TGA, XRD, solution/thin film optical spectroscopy, photoluminescence, and electrochemical measurements. The charge-transporting properties of the oligomers were characterized in FET devices, which reveal that the charge transporting efficiency is significantly enhanced by introducing cycloalkyl substituents at the oligomer silicon atoms. Oligomer **SM5** with two Si-*n*-hexyl substituents is not FET-active, whereas the mobilities of **SM4** and **SM3** FETs are 2.6×10^{-4} and 3.4×10^{-4} $cm^2/(V\,s)$, respectively. These results are also supported by single-crystal structure determinations showing that the intermolecular $\pi-\pi$ packing distances decrease substantially on introducing less encumbered silacycloalkyl substituents, and melting point studies that indicate **SM4** and **SM3** have more dense intermolecular $\pi-\pi$ stacking than **SM5**. The charge transporting properties of the silole-containing copolymers were also studied in FETs. The highest measured mobility was that of copolymer **P4** at 2×10^{-3} $cm^2/V\cdot s$, lower than that of other silole-containing polymers with long Si-alkyl substituents, implying that the solubility and self-assembly functions of alkyl substituents are also important for optimizing the mobility of polymeric semiconductors. These experimental and theoretical results afford better fundamental understanding of the functions of the alkyl substituents in the small molecule and polymeric semiconductors, and provide strategic guidelines for designing high mobility, environmentally stable organic semiconductors.

EXPERIMENTAL SECTION

All reagents were purchased from commercial sources and used without further purification unless otherwise noted. Anhydrous THF was distilled from Na/benzophenone. Conventional Schlenk techniques were used, and reactions were carried out under N2 unless otherwise noted. Optical spectra were recorded on a Cary Model 1 UV−vis spectrophotometer. Fluorescence measurements were recorded on a Photon Technology International model QM-2 fluorimeter. NMR spectra were recorded on a Varian Unity Plus 500 spectrometer (^1H, 500 MHz; ^{13}C, 125 MHz). GPC analyses of polymer samples were performed on a Waters Alliance GPCV 2000 (3 columns, Waters Styragel HT 6E, HT 4, HT 2; operation temperature, 150 °C; mobile phase, 1,2,4-trichlorobenzene or THF at room temperature; flow rate, 1 mL/min) and are reported relative to polystyrene standards purchased from Aldrich. Electrospray mass spectrometry was performed with a Thermo Finnegan model LCQ Advantage mass spectrometer. Electrochemistry was performed on a C3 Cell Stand electrochemical station equipped with BAS Epsilon software (Bioanalytical Systems, Inc., Lafayette, IN).

Synthesis of 3,3′-Cyclopropylsilylene-2,2′-bithiophene (3). A THF (40 mL) solution of dibromo-bithiophene (3.24 g, 10.0 mmol) was added to a dry THF (40 mL) solution of n-BuLi (9 mL, 22.5 mmol) dropwise with vigorous stirring over a period of 30 min. The mixture was then stirred at −78 °C for 1 h. to give a white suspension. A THF (20 mL) solution of dichlorocyclotrimethylsilane (1.6 g, 11.3 mmol) was next added dropwise over 5−10 min. The reaction mixture was stirred at −78 °C and gradually warmed up to room temperature. After stirring overnight, the reaction mixture was quenched with a saturated aqueous NH_4Cl solution (100 mL). The mixture was then extracted with ethyl ether (100 mL × 3), and the organic portions were combined, washed with water (100 mL × 3 times), and dried over $MgSO_4$. After filtration, the solvent was removed by rotary evaporation, and the crude product was purified by column chromatography (silica gel, CH_2Cl_2:hexane = 1:4) to give a light yellow liquid. Yield: 1.41 g, 60%. Anal. Calcd for $C_{11}H_{10}S_2Si$: C, 56.36%; H, 4.30%. Found: C, 57.17%; H, 4.54%. ^1H NMR ($CDCl_3$, 500 MHz, 21 °C): δ 7.24 (d, 2H, J = 5 Hz); 7.19 (d, 2H, J = 5 Hz); 2.39 (hept, 4H, J = 9 Hz); 1.60 (t, 4H, J = 9 Hz). ^{13}C NMR ($CDCl_3$, 125.6 MHz, 21 °C): δ 149.9; 139.4; 129.5; 125.7; 18.9; 15.

Synthesis of 3,3′-Cyclobutylsilylene-2,2′-bithiophene (4). A THF (15 mL) solution of dibromo-bithiophene (1.14 g, 3.5 mmol) was added dropwise to a −78 °C THF (50 mL) solution of n-BuLi (8.5 mmol) dropwise vigorous stirring over a period of 30 min. The mixture was then stirred at −78 °C for 1 h to give a white suspension. Next, a THF (20 mL) solution of dichlorocyclotetramethylsilane was added dropwise over 5−10 min. The reaction mixture was stirred at −78 °C and gradually warmed up to room temperature. After stirring overnight, the reaction mixtue was quenched with saturated aqueous NH_4Cl solution (100 mL). The mixture was then extracted with ethyl ether (100 mL × 3). The organic portions were then combined, washed with water (100 mL × 3 times), and dried over MgSO4. After filtration, the solvent was removed by rotary evaporation, and the crude product was purified by column chromatography (silica gel, CH_2Cl_2:hexane =1:4) to give a light yellow liquid. Yield: 450 mg, 52%. Anal. Calcd for $C_{12}H_{12}S_2Si$: C, 58.01; H, 4.87%. Found: C, 58.70; H, 4.95. ^1H NMR ($CDCl_3$, 500 MHz, 21 °C): δ 7.27 (d, 2H, J = 5 Hz); 7.12 (d, 2H, J = 5 Hz); 1.94 (m, 4H); 1.07 (m, 4H). ^{13}C NMR ($CDCl_3$, 125.6 MHz, 21 °C): δ 149.7; 141.0; 129.4; 125.6; 27.5; 9.65. High-resolution MS: (M + H) 249.0232.

Synthesis of 3,3′-Cyclopentanylsilylene-2,2′-bithiophene (5). A THF (20 mL) solution of dibromo-bithiophene (1.62 g, 5.00 mmol) was added dropwise to a dry −78 °C THF (50 mL) solution of n-BuLi (10 mmol) with vigorous stirring over a period of 30 min. The mixture was then stirred at −78 °C for 1 h to give a white suspension. A THF (20 mL) solution of dichlorocyclopentamethylsilane was next added dropwise in 5−10 min. The reaction mixture was then stirred at −78 °C and gradually warmed up to room temperature. After overnight, the reaction was quenched by saturated aqueous NH_4Cl solution (100 mL). The mixture was then extracted with ethyl ether (100 mL × 3). The organic portions were combined and washed with water (100 mL × 3 times) and dried over MgSO4. After filtration, the solvent was removed, and the crude product was purified by column chromatography (silica gel, CH_2Cl_2:hexane =1:4) to give a light yellow liquid. 600 mg, 46%. Anal. Calcd for $C_{13}H_{14}S_2Si$: C, 59.49; H, 5.38. Found: C, 58.80; H, 5.14. ^1H NMR(C_6D_6, 500 MHz, 25 °C): δ 7.24 (d, 2H, J = 5 Hz); 7.17 (d, 2H, J = 5 Hz); 2.01 (m, 4H); 1.67 (m, 2H); 0.97 (t, 4H, J = 7 Hz). ^{13}C NMR (C_6D_6, 125.7 MHz, 25 °C): δ 149.5; 141.8; 129.7; 124.5; 29.8; 25.2; 11.0

Synthesis of 5,5′-Dibromo-3,3′-cyclobutylsilylene-2,2′-bithiophene (7). NBS (1.35 g, 7.56 mmol) was added to a DMF (20 mL) solution of **4** (750 mg, 3.02 mmol) in one portion. The mixture was stirred at room temperature overnight to give a brownish-yellow solution, which was quenched with water (50 mL). The mixture was then extracted with ether (200 mL × 3) to give a yellow ether solution, which was dried over $MgSO_4$ overnight. After filtration, the solvent was removed by rotary evaporation to give a brownish-yellow solid. The crude product was purified by column chromatography using hexane as eluent to give a yellow solution. The solvent was removed to give a light yellow solid, which was recrystallized from hexane to give light yellow crystals. Yield: 1.13 g, 92%; Anal. Calcd for $C_{12}H_{10}Br_2S_2Si$: C, 35.48; H, 2.48; S, 15.79. Found: C, 35.59; H, 2.54; S, 15.63. ^1H NMR (C_6D_6, 300 MHz, 25 °C): δ 7.02 (2H, s); 1.85 (4H, m); 0.99 (4H, t, J = 7 Hz). ^{13}C NMR (C_6D_6, 125.7 MHz, 25 °C): δ 149.3; 140.2; 131.9; 111.8; 27.3; 9.39.

Synthesis of 5,5′-Dibromo-3,3′-cyclopentanylsilylene-2,2′-bithiophene (8). NBS (1.07 g, 6.00 mmol) was added to a

DMF (20 mL) solution of **5** (600 mg, 2.29 mmol) in one portion. The mixture was then stirred at room temperature overnight to give a brownish-yellow solution, which was quenched with water (50 mL). The mixture was then extracted with ether (200 mL × 3) to give a yellow solution, which was dried over $MgSO_4$ overnight. After filtration, the solvent was removed by rotary evaporation to give a brownish-yellow solid. The crude product was purified by column chromatography (silica gel) using hexane as eluent to give a yellow solution. The solvent was removed to give a light yellow solid, which was recrystallized from hexane to give a light yellow solid. Yield: 900 mg, 94%. Anal. Calcd for $C_{13}H_{12}Br_2S_2Si$: C, 37.15; H, 2.88; S, 15.26. Found: C, 37.46; H, 2.93; S, 14.90. ^{1}H NMR(C_6D_6, 300 MHz, 25 °C): δ 7.09 (2H, s); 1.94 (4H, m); 1.62 (2H, m); 0.92 (4H, t, J = 7 Hz). ^{13}C NMR (C_6D_6, 125.7 MHz, 25 °C): δ 149.1; 140.8; 132.2; 111.6; 29.4; 25.4; 10.9.

Synthesis of 5″,5‴-Dihexyl-3,3′-cyclopentanylsilylene-2,2′:5,2″:5′,2‴:5″,2‴-tetrathiophene (SM1). A toluene (20 mL) solution of dibromothiophene **8** (264 mg, 0.63 mmol), hexyl-trimethyltinthiophene (417 mg, 1.26 mmol), and $Pd(PPh_3)_2Cl_2$ (5 mg) was refluxed under N_2 overnight to give a red solution. The reaction mixture was quenched with water (50 mL), and extracted with CH_2Cl_2 (200 mL × 2). The organic portions were combined, washed with water (200 mL × 2), and dried over $MgSO_4$ overnight. After filtration, the solvent was evaporated to give a dark red oil, which was purified by column chromatography (silica gel, CH_2Cl_2:hexane =1:10) to give a red solution. The solvent was removed to give dark red oil. Yield: 300 mg, 80%. Anal. Calcd $C_{33}H_{42}S_4Si$: C, 66.61; H, 7.11. Found: C, 67.01; H, 7.20. ^{1}H NMR ($CDCl_3$, 500 MHz, 21 °C): δ 7.14 (2H, d, J = 5 Hz); 6.97 (2H, d, J = 5 Hz; 6.69 (2H, s); 2.81 (4H, t, J = 7 Hz); 2.00 (4H, m); 1.70 (6H, m); 1.41−1.28 (m, 12H); 0.99−0.92 (m, 10H). MALDI: 594.2 (100%); 595.2 (36.2%); 596.2 (21.6%).

Synthesis of 5‴″,5‴″-Dihexyl-3,3′-cyclopentanylsilylene-2,2′:5,2″:5′,2‴:5″,2‴″:5‴,2‴″-sexithiophene (SM2). A toluene solution (20 mL) of dibromothiophene **8** (420 mg, 1.00 mmol), hexyl-trimethyltinbithiophene (826 mg, 2.00 mmol), and $Pd(PPh_3)_2Cl_2$ (5 mg) was refluxed under N_2 overnight to give a red solution. The reaction mixture was then quenched with water (50 mL). The mixture was extracted with CH_2Cl_2 (200 mL × 2) and the organic portions were combined, washed with water (200 mL × 2), and dried over $MgSO_4$ overnight. After filtration, the solvent was evaporated to give a dark red solid, which was purified by column chromatography (silica gel, CH_2Cl_2: hexane =1:4) to give a red solution. The solvent was removed to give a dark red solid. Yield: 600 mg, 79%. Anal. Calcd $C_{41}H_{46}S_6Si$: C, 64.86; H, 6.11; S, 25.34. Found: C, 64.62; H, 6.20; S 24.80. ^{1}H NMR ($CDCl_3$, 500 MHz, 21 °C): δ 7.19 (2H, s); 7.04 (2H, d, J = 4 Hz); 7.01 (2H, d, J = 4 Hz); 6.99 (2H, d, J = 4 Hz); 6.70 (2H, d, J = 4 Hz); 2.81 (4H, t, J = 8 Hz); 2.00 (4H, m); 1.68 (6H, m); 1.41−1.32 (12H, m); 1.00−0.92 (10H, m). ^{13}C NMR (C_6D_6, 125.7 MHz, 25 °C): δ 146.7; 144.6; 141.8; 137.2; 135.4; 134.5; 133.5; 135.2; 125.2; 123.8; 122.9; 122.6; 122.2. Mp: 144−146 °C.

Synthesis of 3,3′-Cyclobutylsilylene-2,2′:5,2″:5′,2‴:5″,2‴″:5‴,2‴″-sexithiophene (SM3). A DMF (5 mL) solution of dibromothiophene **7** (102 mg, 0.25 mmol), trimethyltin bithiophene (165 mg, 0.51 mmol), and $Pd(PPh_3)_2Cl_2$ (5 mg) was heated at 90 °C overnight. After cooling to room temperature, a large amount of orange precipitate was obtained, which was collected by filtration and washed with hexane to give an orange solid. Yield: 80 mg, 55%. Anal. Calcd $C_{28}H_{20}S_6Si$: C, 58.29; H, 3.49. Found: C, 58.21; H, 3.59. ^{1}H NMR ($CDCl_3$, 500 MHz, 21 °C): δ 7.23 (2H, d, J = 5 Hz); 7.18 (d, 4 Hz); 7.14 (2H, s);7.09 (2H, d, J = 4 Hz); 7.06 (2H, d, J = 4 Hz); 7.03 (2H, q, d = 4 Hz); 1.89 (4H, m, $2CH_2$); 1.06 (4H, m, $2CH_2$). ^{13}C NMR (C_6D_6, 125.7 MHz, 25 °C): δ 148.1; 142.3; 138.4; 137.1; 136.2; 135.8; 127.9; 126.1; 124.5; 124.4; 123.9; 123.6; 27.4; 9.59. Mp: 236−238 °C.

Synthesis of 3,3′-Cyclopentanylsilylene-2,2′:5,2″:5′,2‴:5″,2‴:5‴,2‴″-sexithiophene (SM4). A DMF solution (12 mL) of dibromothiophene **8** (105 mg, 0.25 mmol), trimethyltin bithiophene (165 mg, 0.51 mmol), and $Pd(PPh_3)_2Cl_2$ (5 mg) was heated at 90 °C. After 1 h, an orange precipitate formed. After continuing overnight, a large quantity of orange precipitate was obtained, which was collected by filtration and washed with hexane to give an orange solid. Yield: 100 mg, 69%.; Anal. Calcd for $C_{29}H_{22}S_6Si$: C, 58.94; H, 3.75; S, 32.56. Found: C, 58.86; H, 3.87; S, 32.36. ^{1}H NMR ($CDCl_3$, 500 MHz, 21 °C) δ 7.23 (2H, d, J = 5 Hz); 7.22 (2H, s); 7.19 (d, J = 4 Hz); 7.10 (2H, d, J = 4 Hz); 7.08 (2H, d, J = 4 Hz); 7.04 (2H, q, d = 4 Hz); 2.01 (4H, m, $2CH_2$); 1.67 (2H, m, CH_2); 1.00 (4H, t, J = 6 Hz, $2CH_2$). ^{13}C NMR (C_6D_6, 125.7 MHz, 25 °C) δ 147.9; 143.0; 138.1; 137.2; 136.2; 135.9; 128.0; 126.4; 124.5; 124.4; 124.0; 123.6; 29.; 25.5; 11.1. Mp: 244−246 °C.

Synthesis of 3,3′-Dihexylsilylene-2,2′:5,2″:5′,2‴:5″,2‴″:5‴,2‴″-sexithiophene (SM5). A DMF (2 mL) solution of bistributylthiophene (200 mg, 0.200 mmol), bromobithiophene **9** (98 mg, 0.400 mmol), and $Pd(PPh_3)_2Cl_2$ (10 mg) was heated at 90 °C. After continuing overnight, a dark red solution was obtained. The solvent was removed under vacuo to give a dark red oil, which was purified by column chromatography (silica gel, CH_2Cl_2:hexane = 1:3) to give a red solution. The solvent was removed to give dark red oil, which was recrystallized from hexane to give a dark red solid. Yield, 100 mg, 85%. Anal. Calcd for $C_{36}H_{38}S_6Si$: C, 62,56; H, 5.54. Found: C, 62.35; H, 5.63. ^{1}H NMR ($CDCl_3$, 500 MHz, 21 °C): δ 7.24 (2H, d, J = 5 Hz); 7.19 (d, J = 4 Hz); 7.14 (2H, s); 7.09 (2H, d, J = 4 Hz); 7.06 (2H, d, J = 4 Hz); 7.04 (2H, q, d = 4 Hz); 1.21−1.41 (16H, m); 0.86−0.96 (10H, m). ^{13}C NMR (C_6D_6, 125.7 MHz, 25 °C): δ 147.7; 143.2; 137.9; 137.2; 136.4; 135.7; 127.9; 126.4; 124.6; 124.4; 123.8; 123.6; 32.9; 31.4; 24.1; 22.6; 14.1; 11.8. Mp: 134−136 °C.

Synthesis of P1. A THF solution (40 mL) of dibromothiophene **8** (280 mg, 0.67 mmol), bistrimethyltinthiophene (278 mg, 0.67 mmol), and $Pd(PPh_3)_2Cl_2$ (2 mg) was refluxed under N_2 for 7 days to give a dark purple solution. The reaction mixture was then cooled to room temperature and poured into methanol (500 mL). The resulting black solid was collected by filtration. The black solid was dissolved in THF again and precipitated with methanol, and this procedure was repeated twice more to give a dark brown solid. 200 mg, 87%. M_w, 4.9 KDa; PDI, 1.13; Anal. Calcd for $C_{18}H_{14}S_3Si$: C, 59.60; H 4.12. Found: C, 60.31; H, 6.50. ^{1}H NMR ($C_2D_2Cl_4$, 400 MHz, 25 °C): δ 7.24 (2H, brm, ArH); 7.11 (2H, brm, ArH); 2.01 (4H, brm, $2CH_2$); 1.61 (2H, brm, CH_2); 1.01 (4H, brm, $2CH_2$).

Synthesis of P2. A THF solution (50 mL) of dibromothiophene **8** (420 mg, 1.00 mmol), 5,5′-bis(trimethylstannyl)-2,2′-bithiophene (492 mg, 1.00 mmol), and $Pd(PPh_3)_4$ (40 mg) was refluxed under N_2 for 5 days to give a purple solution. The mixture was then poured into methanol (500 mL), and the resulting precipitate collected and subjected to Soxhlet extraction with methanol, ethyl acetate, 1,4-dioxane, and chloroform, each for 1 day. The remaining dark red solid was dried under a vacuum. Yield: 200 mg, 59%. Anal. Calcd for $C_{21}H_{16}S_4Si$: C, 59.39; H, 3.80. Found: C, 57.10; H, 3.63. ^{1}H NMR ($C_2D_2Cl_4$, 400 MHz, 100 °C): δ 7.32 (2H, brm, ArH); 7.28 (2H, brm, ArH); 7.16 (2H, brm, CH_2); 2.07 (4H, brm,$2CH_2$); 1.67 (2H, brm, CH_2); 1.08 (4H, brm, $2CH_2$).

Synthesis of P3. A toluene solution (20 mL) of bithiophene **8** (90 mg, 0.21 mmol), 3,3′-dodecoxy-5,5′-bis(trimethylstannane)-2,2′-bithiophene (185 mg, 0.21 mmol), and $Pd(PPh_3)_2Cl_2$ (2 mg) was heated at 95 °C for 2 days and then cooled to room temperature. The mixture was next poured into a mixture of methanol (500 mL) and HCl (5 mL, 12 M). The mixture was stirred at room temperature for 4 h and then filtered to give a dark purple solid. The solid was then subjected to Soxhlet extraction with methanol, acetone, ethyl acetate, each for 1 day. The solid was extracted with $CHCl_3$ and concentrated, and then added to methanol (500 mL) dropwise to give a dark blue precipitate, which was collected by filtration and dried under a vacuum to give a metallic dark blue solid. Yield: 100 mg, 71%. M_w, 32 KDa; PDI, 6.0. Anal. Calcd for $C_{45}H_{66}O_2S_4Si$: C, 68.13; H, 8.13. Found: C, 67.44; H, 8.01. ^{1}H NMR ($CHCl_3$, 500 MHz, 25 °C): δ 6.94 (2H, brm, ArH); 6.93 (2H, brm, ArH); 4.19 (4H, brm, CH_2); 2.01 (4H, brm, CH_2); 1.93 (4H, brm, CH_2); 1.59−1.25 (36H, brm, CH_2); 0.89−0.87 (10H, brm, CH_2+CH_3). ^{13}C

NMR ($CHCl_3$, 125.7 MHz, 25 °C): δ 150.95; 146.5; 141.8; 138.1; 137.3; 131.7; 125.0; 124.2; 112.4; 111.0; 110.3;.71.1; 30.9; 30.6; 28.7; 28.5; 28.4; 28.3; 25.2; 25.2; 24.5; 21.7; 21.6; 13.1; 10.1.

Synthesis of P4. A toluene solution (15 mL) of bibromobithiophene **8** (105 mg, 0.25 mmol), 2,6-bis(trimethyltin)-4,8-dioctylbenzo[1,2-*b*:4,5-*b*′]dithiophene (185 mg, 0.25 mmol), and $Pd(PPh_3)_2Cl_2$ (2 mg) was heated at 110 °C under N_2 for 2 days. The reaction mixture was then cooled to room temperature and poured into a mixture of methanol (500 mL) and HCl (5 mL, 12M). This mixture was stirred for 4 h and then filtered to give a dark purple solid. Crude yield, 160 mg. The solid was subjected to Soxhlet extraction with methanol, acetone, ethyl acetate, each for one day, and $CHCl_3$ for 3 days. The residual solid was dissolved in dichlorobenzene and added to methanol (100 mL) to precipitate it. The product was next collected by filtration. Yield: 100 mg, 52%. Anal. Calcd for $C_{39}H_{50}S_4Si$: C, 69.00; H, 7.20. Found: C, 69.00; H, 7.40. ^1H NMR ($C_2D_2Cl_4$, 400 MHz, 100 °C): δ 7.5−7.32 (4H, brm, ArH); 3.24 (4H, brm, CH_2−Ar); 2.13−1.46 (34H, brm, 17CH_2); 1.00 (6H, brm, 2CH_3)

Synthesis of P5. A toluene solution (5 mL) of bithiophene **8** (140 mg, 0.24 mmol), *N*,*N*′-bis(2-octyldodecyl)- 1,4,5,8-naphthalenedicarboximide (220 mg, 0.24 mmol), and $Pd(PPh_3)_2Cl_2$ (2 mg) was heated at 95 °C for 2 days and then cooled to room temperature. The mixture was then poured into a mixture of methanol (500 mL) and HCl (5 mL, 12 M). This mixture was stirred at room temperature for 4 h and then filtered to give a dark purple solid. The solid was subjected to Soxhlet extraction with methanol, acetone, ethyl acetate, each for 1 day. The solid was then extracted with $CHCl_3$, concentrated, and then added to methanol (500 mL) dropwise to give a dark blue precipitate, which was collected by filtration and dried under a vacuum to give a metallic dark blue solid. Yield: 200 mg, 80%. M_w, 18 KDa; PDI, 2.26. Anal. fCalcd or $C_{67}H_{96}O_4S_4Si$: C, 74.12; H, 9.09. Found: C, 73.77; H, 8.61. ^1H NMR($CHCl_3$, 500 M, 25 °C): 8.78 (2H, brm, ArH); 7.44 (2H, brm, AH); 4.06 (4H, brm, 2CH_2−N); 1.99 (8H, brm, 4CH_2); 1.55 (4H, brm, 2CH_2); 1.28 (84H, brm, 42CH_2); 0.78 (12H, brm, 4CH_3); ^{13}C NMR ($CHCl_3$, 125.7 MHz, 25 °C): δ 162.2; 161.9; 151.7; 142.3; 141.7; 138.5; 135.8; 131.3; 126.6; 142.2; 120.8.

Single-Crystal Structure Determinations. Single crystals of **SM3**, **SM4**, and **SM5** were grown by slow diffusion of hexane into dichlorobenzene solution. X-ray single crystal diffraction measurements were performed on a Bruker CCD area detector instrument with graphite-monochromated MoKα (0.71073 A) radiation. The data were collected at 153(2)K, and the structures were solved by direct methods and expanded using Fourier techniques.

Device Fabrication and Thin-Film Characterization. *Oligomers.* Thin film transistors were fabricated in the bottom-gate/top-contact configuration. Highly doped p-type (100) silicon wafers (<0.004 Ω cm) were used as gate electrodes as well as substrates, and 300 nm SiO_2 thermally grown on Si was used as the gate insulator. The unit area capacitance is 11 nF/cm^2. The substrate surface was treated with octadecyltrichlorosilane-(OTS) and hexamethyldisilazane (HMDS) purchased from Aldrich. A few drops of HMDS were loaded inside a self-assembly chamber under an N_2 blanket. The SiO_2/Si substrates were exposed to this atmosphere for at least 7.0 days to give a hydrophobic surface. After HMDS deposition, the advancing aqueous contact angle is 95°. OTS was deposited under an N_2 blanket inside a self-assembly chamber. The SiO_2/Si substrates were exposed to ethanol solution for 10 h to give a hydrophobic surface. After OTS deposition, the advancing aqueous contact angle is 105°. Semiconductor thin films (50 nm) were next vapor-deposited onto the Si/SiO_2 held at well-defined temperatures of 25 or 80 °C with a deposition rate of 0.3 Å/s at 6×10^{-6} Torr, employing a high-vacuum deposition chamber (Denton Vacuum, Inc., USA). Gold source and drain electrodes (50 nm) were vapor-deposited at 2×10^{-6} Torr through a shadow mask in the vacuum deposition chamber. Devices were fabricated with typical channel lengths of 50 and100 μm, and a channel width of 2000 μm.

Polymers. For **P1**−**P4**, OTFTs were fabricated on glass substrates (Precision Glass & Optics, Eagle 2000). Gold source and drain electrodes (30 nm) were deposited by thermal evaporation with a W/L ratio of 10. Semiconductors were prepared as 7 mg/mL solutions in 1,2-dichlorobenzene and were filtered through a 0.22 μm PTFE syringe filter. The semiconductor films were deposited by spincoating at 1500 rpm and annealed in a vacuum oven maintained at 110 or 190 °C for 2 h. For the dielectric, 400−500 nm thick PMMA (Aldrich, M_w 350K) films were spuncoat on top of the semiconductor film. The dielectric films are dried in a 110 °C vacuum oven for 2 h, and 30 nm gold films were then deposited by thermal evaporation as the gate electrode. For **P5**, thin film semiconductor layers were deposited by spin-coating of a 10 mg/mL polymer solution in chloroform under ambient conditions onto hexamethyldisilazane (HMDS)-treated p-doped Si (001) wafers with a 300 nm thermally grown SiO_2 dielectric layer. The capacitance of the 300 nm SiO_2 gate insulator was 11 nFcm^{-2}. Prior to the semiconductor deposition, the wafers were solvent cleaned by sonicating (in two beakers, sequentially, for 30 s each) in EtOH and were then dried with a filtered stream of nitrogen, followed by 5 min plasma cleaning in a Harrick PDC-32G Plasma Cleaner/Sterilizer. After semiconductor deposition, the films were annealed either at 150 °C under in vacuum for 30 min or at 200 °C under nitrogen for 1 h. Top-contact OTFTs were fabricated by vapor deposition of gold electrodes ($\sim 1 \times 10^{-7}$ Torr, 0.2 Å/s, ∼50 nm thick) onto the semiconductor thin films through a shadow mask to obtain devices with channel widths and lengths of 5000 and 100 μm, respectively.

OTFT Characterization. *I*−*V* plots of device performance were measured under vacuum, and transfer and output plots were recorded for each device. The current−voltage (*I*−*V*) characteristics of the devices were measured using a Keithley 6430 subfemtoammeter and a Keithly 2400 source meter, operated by a local Labview program and GPIB communication. Key device parameters, such as charge carrier mobility (μ) and on-to-off current ratio (I_{on}/I_{off}), were extracted from the source-drain current (I_{SD}) versus source-gate voltage (V_{SG}) characteristics employing standard procedures. Mobilities were obtained from the formula defined by the saturation regime in transfer plots, $\mu = 2I_{SD}L/[C_iW(V_{SG} - V_T)^2]$, where I_{SD} is the source-drain current, V_{SG} is source-gate voltage, and V_T is the threshold voltage. Threshold voltage was obtained from x intercept of V_{SG} vs $I_{SD}^{1/2}$ plots. AFM measurements were performed by using a JEOL-Microscope (JEOL Ltd. Japan) in the tapping mode.

Electrochemistry. Cyclic voltammetry was performed in an electrolyte solution of 0.1 M tetrabutylammonium hexafluorophosphate ($Bu_4N^+PF_6^-$) in dry acetonitrile. Platinum wire electrodes were used as both working and counter electrodes, and Ag wire was used as the pseudoreference electrode. A ferrocene/ferrocenium redox couple was used as an internal standard, and potentials obtained in reference to a silver electrode were converted to the saturated calomel electrode (SCE) scale. Thin films of the polymers were coated onto the Pt working electrode by drop-casting from 0.5 to 1.0 wt % THF solutions and dried under a vacuum at 80 °C for 2 h.

Electronic Structure Calculations. DFT calculations were carried out using the Gaussian 03 program.[91] Becke's three-parameter exchange functional combined with the LYP correlation functional (B3LYP)[92] was employed. We also made use of the standard 6-31G** basis set.[93] Vertical electronic excitation energies were computed using the time−dependent DFT (TDDFT) approach.[94−97] The twelve lowest-energy electronic excited states were computed for molecules **SM3**, **SM4**, and **SM5**. TDDFT calculations were carried out using the B3LYP functional and the 6-31G** basis set on the previously optimized molecular geometries obtained at the same level of calculation.

AUTHOR INFORMATION

Corresponding Author

*To whom correspondence should be addressed. E-mail: Prof. Antonio Facchetti (email: a-facchetti@northwestern.edu), Prof. Tobin J. Marks (email: t-marks@northwestern.edu).

■ ACKNOWLEDGMENT

We thank Polyera Corp. and ONR AFOSR (FA9550-08-1-0331) for support of this research at Northwestern University. We thank the NSF-MRSEC program through the Northwestern Materials Research Center (DMR-0520513) for support of characterization facilities. The research leading to these results has received funding from the European Community's Seventh Framework Programme under Grant Agreement 234808.

■ REFERENCES

(1) Braga, D.; Horowitz, G. *Adv. Mater.* **2009**, *21*, 1473.
(2) Murphy, A. R.; Frechet, J. M. J. *Chem. Rev.* **2007**, *107*, 1066.
(3) Dimitrakopoulos, C. D.; Malenfant, P. R. L. *Adv. Mater.* **2002**, *14*, 99.
(4) Facchetti, A. *Mater. Today* **2007**, *10*, 28.
(5) Zhang, W.; Smith, J.; Watkins, S. E.; Gysel, R.; McGehee, M.; Salleo, A.; Kirkpatrick, J.; Ashraf, S.; Anthopoulos, T.; Heeney, M.; McCulloch, I. *J. Am. Chem. Soc.* **2010**, *132*, 11437.
(6) Kim, D. H.; Lee, B.-L.; Moon, H.; Kang, H. M.; Jeong, E. J.; Park, J.-I.; Han, K.-M.; Lee, S.; Yoo, B. W.; Koo, B. W.; Kim, J. Y.; Lee, W. H.; Cho, K.; Becerril, H. A.; Bao, Z. *J. Am. Chem. Soc.* **2009**, *131*, 6124.
(7) Osaka, I.; Abe, T.; Shinamura, S.; Miyazaki, E.; Takimiya, K. *J. Am. Chem. Soc.* **2010**, *132*, 5000.
(8) Osaka, I.; Zhang, R.; Sauve, G.; Smilgies, D.-M.; Kowalewski, T.; McCullough, R. D. *J. Am. Chem. Soc.* **2009**, *131*, 2521.
(9) Hwang, S.-H.; Moorefield, C. N.; Newkome, G. R. *Chem. Soc. Rev.* **2008**, *37*, 2543.
(10) Burn, P. L.; Lo, S.-C.; Samuel, I. D. W. *Adv. Mater.* **2007**, *19*, 1675.
(11) Dennler, G.; Scharber, M. C.; Brabec, C. J. *Adv. Mater.* **2009**, *21*, 1323.
(12) Thompson, B. C.; Frechet, J. M. J. *Angew. Chem., Int. Ed.* **2008**, *47*, 58.
(13) Guenes, S.; Neugebauer, H.; Sariciftci, N. S. *Chem. Rev.* **2007**, *107*, 1324.
(14) Nelson, J. *Science* **2001**, *293*, 1059.
(15) Fichou, D.; Horowitz, G.; Nishikitani, Y.; Garnier, F. *Chemtronics* **1988**, *3*, 176.
(16) Horowitz, G.; Fichou, D.; Peng, X.; Xu, Z.; Garnier, F. *Solid State Commun.* **1989**, *72*, 381.
(17) Peng, X.; Horowitz, G.; Fichou, D.; Garnier, F. *Appl. Phys. Lett.* **1990**, *57*, 2013.
(18) Facchetti, A.; Yoon, M.-H.; Stern, C. L.; Katz, H. E.; Marks, T. J. *Angew. Chem., Int. Ed.* **2003**, *42*, 3900.
(19) Facchetti, A.; Yoon, M.-H.; Stern, C. L.; Hutchison, G. R.; Ratner, M. A.; Marks, T. J. *J. Am. Chem. Soc.* **2004**, *126*, 13480.
(20) Facchetti, A.; Mushrush, M.; Yoon, M.-H.; Hutchison, G. R.; Ratner, M. A.; Marks, T. J. *J. Am. Chem. Soc.* **2004**, *126*, 13859.
(21) Katz, H. E.; Bao, Z.; Gilat, S. L. *Acc. Chem. Res.* **2001**, *34*, 359.
(22) Garnier, F.; Hajlaoui, R.; Yassar, A.; Srivastava, P. *Science* **1994**, *265*, 1864.
(23) Rogers, J. A.; Bao, Z.; Baldwin, K.; Dodabalapur, A.; Crone, B.; Raju, V. R.; Kuck, V.; Katz, H.; Amundson, K.; Ewing, J.; Drzaic, P. *Proc. Natl. Acad. Sci. U.S.A.* **2001**, *98*, 4835.
(24) Sirringhaus, H.; Kawase, T.; Friend, R. H.; Shimoda, T.; Inbasekaran, M.; Wu, W.; Woo, E. P. *Science* **2000**, *290*, 2123.
(25) Bao, Z.; Dodabalapur, A.; Lovinger, A. J. *Appl. Phys. Lett.* **1996**, *69*, 4108.
(26) Bao, Z.; Lovinger, A. J. *Chem. Mater.* **1999**, *11*, 2607.
(27) Sirringhaus, H.; Brown, P. J.; Friend, R. H.; Nielsen, M. M.; Bechgaard, K.; Langeveld-Voss, B. M. W.; Spiering, A. J. H.; Janssen, R. A. J.; Meijer, E. W.; Herwig, P.; De Leeuw, D. M. *Nature* **1999**, *401*, 685.
(28) Colomer, E.; Corriu, R. J. P.; Lheureux, M. *Chem. Rev.* **1990**, *90*, 265.
(29) Tamao, K.; Yamaguchi, S.; Shiro, M. *J. Am. Chem. Soc.* **1994**, *116*, 11715.
(30) Zhan, X.; Risko, C.; Amy, F.; Chan, C.; Zhao, W.; Barlow, S.; Kahn, A.; Bredas, J.-L.; Marder, S. R. *J. Am. Chem. Soc.* **2005**, *127*, 9021.
(31) Tamao, K.; Uchida, M.; Izumizawa, T.; Furukawa, K.; Yamaguchi, S. *J. Am. Chem. Soc.* **1996**, *118*, 11974.
(32) Yamaguchi, S.; Goto, T.; Tamao, K. *Angew. Chem., Int. Ed.* **2000**, *39*, 1695.
(33) Zhan, X.; Haldi, A.; Risko, C.; Chan, C. K.; Zhao, W.; Timofeeva, T. V.; Korlyukov, A.; Antipin, M. Y.; Montgomery, S.; Thompson, E.; An, Z.; Domercq, B.; Barlow, S.; Kahn, A.; Kippelen, B.; Bredas, J.-L.; Marder, S. R. *J. Mater. Chem.* **2008**, *18*, 3157.
(34) Yamaguchi, S.; Tamao, K. *Bull. Chem. Soc. Jpn.* **1996**, *69*, 2327.
(35) Chan, K. L.; McKiernan, M. J.; Towns, C. R.; Holmes, A. B. *J. Am. Chem. Soc.* **2005**, *127*, 7662.
(36) Chen, J.; Law, C. C. W.; Lam, J. W. Y.; Dong, Y.; Lo, S. M. F.; Williams, I. D.; Zhu, D.; Tang, B. Z. *Chem. Mater.* **2003**, *15*, 1535.
(37) Murata, H.; Kafafi, Z. H.; Uchida, M. *Appl. Phys. Lett.* **2002**, *80*, 189.
(38) DiCarmine, P. M.; Wang, X.; Pagenkopf, B. L.; Semenikhin, O. A. *Electrochem. Commun.* **2008**, *10*, 229.
(39) Hou, J.; Chen, H.-Y.; Zhang, S.; Li, G.; Yang, Y. *J. Am. Chem. Soc.* **2008**, *130*, 16144.
(40) Huo, L.; Chen, H.-Y.; Hou, J.; Chen, T. L.; Yang, Y. *Chem. Commun.* **2009**, 5570.
(41) Mi, B.; Dong, Y.; Li, Z.; Lam Jacky, W. Y.; Haussler, M.; Sung Herman, H. Y.; Kwok Hoi, S.; Dong, Y.; Williams Ian, D.; Liu, Y.; Luo, Y.; Shuai, Z.; Zhu, D.; Tang Ben, Z. *Chem. Commun.* **2005**, 3583.
(42) Wang, F.; Luo, J.; Yang, K.; Chen, J.; Huang, F.; Cao, Y. *Macromolecules* **2005**, *38*, 2253.
(43) Ohshita, J.; Lee, K.-H.; Hamamoto, D.; Kunugi, Y.; Ikadai, J.; Kwak, Y.-W.; Kunai, A. *Chem. Lett.* **2004**, *33*, 892.
(44) Usta, H.; Lu, G.; Facchetti, A.; Marks, T. J. *J. Am. Chem. Soc.* **2006**, *128*, 9034.
(45) Chen, J.; Cao, Y. *Macromol. Rapid Commun.* **2007**, *28*, 1714.
(46) Lu, G.; Usta, H.; Risko, C.; Wang, L.; Facchetti, A.; Ratner, M. A.; Marks, T. J. *J. Am. Chem. Soc.* **2008**, *130*, 7670.
(47) Wang, Y.; Hou, L.; Yang, K.; Chen, J.; Wang, F.; Cao, Y. *Macromol. Chem. Phys.* **2005**, *206*, 2190.
(48) Usta, H.; Facchetti, A.; Marks, T. J. *J. Am. Chem. Soc.* **2008**, *130*, 8580.
(49) Usta, H.; Risko, C.; Wang, Z.; Huang, H.; Deliomeroglu, M. K.; Zhukhovitskiy, A.; Facchetti, A.; Marks, T. J. *J. Am. Chem. Soc.* **2009**, *131*, 5586.
(50) Yan, H.; Chen, Z.; Zheng, Y.; Newman, C.; Quinn, J. R.; Dotz, F.; Kastler, M.; Facchetti, A. *Nature* **2009**, *457*, 679.
(51) Liang, Y.; Feng, D.; Wu, Y.; Tsai, S.-T.; Li, G.; Ray, C.; Yu, L. *J. Am. Chem. Soc.* **2009**, *131*, 7792.
(52) Chen, Z.; Zheng, Y.; Yan, H.; Facchetti, A. *J. Am. Chem. Soc.* **2009**, *131*, 8.
(53) Kim, K. H.; Chi, Z.; Cho, M. J.; Jin, J.-I.; Choi, D. H.; Paek, S. H. *Macromol. Symp.* **2007**, *249/250*, 1.
(54) Chen, S. H.; Zhu, Y.; Jenekhe, S. A.; Su, A. C.; Chen, S. A. *J. Phys. Chem. B* **2007**, *111*, 12345.
(55) Garnier, F.; Yassar, A.; Hajlaoui, R.; Horowitz, G.; Deloffre, F.; Servet, B.; Ries, S.; Alnot, P. *J. Am. Chem. Soc.* **1993**, *115*, 8716.
(56) Videlot, C.; Ackermann, J.; Blanchard, P.; Raimundo, J.-M.; Frere, P.; Allain, M.; de Bettignies, R.; Levillain, E.; Roncali, J. *Adv. Mater.* **2003**, *15*, 306.
(57) Coropceanu, V.; Cornil, J.; da Silva Filho Demetrio, A.; Olivier, Y.; Silbey, R.; Bredas, J.-L. *Chem. Rev.* **2007**, *107*, 926.
(58) Bredas, J.-L.; Beljonne, D.; Coropceanu, V.; Cornil, J. *Chem. Rev.* **2004**, *104*, 4971.
(59) Minari, T.; Seto, M.; Nemoto, T.; Isoda, S.; Tsukagoshi, K.; Aoyagi, Y. *Appl. Phys. Lett.* **2007**, *91*, 123501/1.
(60) Son, H.-J.; Han, W.-S.; Chun, J.-Y.; Kwon, S.-N.; Ko, J.; Kang, S. O. *Organometallics* **2008**, *27*, 2464.
(61) Son, H.-J.; Han, W.-S.; Chun, J.-Y.; Lee, C.-J.; Han, J.-I.; Ko, J.; Kang, S. O. *Organometallics* **2007**, *26*, 519.
(62) Baumgartner, T.; Bergmans, W.; Karpati, T.; Neumann, T.; Nieger, M.; Nyulaszi, L. *Chem.—Eur. J.* **2005**, *11*, 4687.

(63) Roncali, J. *Acc. Chem. Res.* **2000**, *33*, 147.
(64) Zhu, Y.; Alam, M. M.; Jenekhe, S. A. *Macromolecules* **2002**, *35*, 9844.
(65) Hernandez, V.; Lopez, N. J. T. *J. Chem. Phys.* **1994**, *101*, 1369.
(66) Nueesch, F.; Graetzel, M. *Chem. Phys.* **1995**, *193*, 1.
(67) Reimers Jeffrey, R.; Cai, Z.-L.; Bilic, A.; Hush Noel, S. *Ann. N.Y. Acad. Sci.* **2003**, *1006*, 235.
(68) Mani, A.; Schoonman, J.; Goossens, A. *J. Phys. Chem. B* **2005**, *109*, 4829.
(69) Chen, T.-A.; Wu, X.; Rieke, R. D. *J. Am. Chem. Soc.* **1995**, *117*, 233.
(70) Guo, X.; Watson, M. D. *Org. Lett.* **2008**, *10*, 5333.
(71) Pope, M.; Swenberg, C. E. *Electronics Processes in Organic Crystals*; Oxford University Press: New York, 1982.
(72) Mikroyannidis, J. A.; Barberis, V. P.; Vyprachticky, D.; Cimrova, V. *J. Polym. Sci., Part A: Polym. Chem.* **2007**, *45*, 809.
(73) Ng, S.-C.; Ong, T.-T.; Chan, H. S. O. *J. Mater. Chem.* **1998**, *8*, 2663.
(74) Heun, S.; Baessler, H.; Mueller, U.; Muellen, K. *J. Phys. Chem.* **1994**, *98*, 7355.
(75) Leclerc, M.; Roux, C.; Bergeron, J. Y. *Synth. Met.* **1993**, *55*, 287.
(76) Wong, W.-Y.; Wong, C.-K.; Poon, S.-Y.; Lee, A. W. M.; Mo, T.; Wei, X. *Macromol. Rapid Commun.* **2005**, *26*, 376.
(77) Jenekhe, S. A.; Osaheni, J. A. *Science* **1994**, *265*, 765.
(78) Prieto, I.; Teetsov, J.; Fox, M. A.; Vanden Bout, D. A.; Bard, A. J. *J. Phys. Chem. A* **2001**, *105*, 520.
(79) Berlaman, I. B. *Handbook of Fluorescence Spectra of Aromatic Molecules*; Academic Pess.: New York, 1971.
(80) Turro, N. J. *Modern Molecular Photochemistry*; University Science Books: Sausalito, CA, 1991.
(81) Zhu, Y.; Champion, R. D.; Jenekhe, S. A. *Macromolecules* **2006**, *39*, 8712.
(82) Chua, L.-L.; Zaumseil, J.; Chang, J.-F.; Ou, E. C. W.; Ho, P. K. H.; Sirringhaus, H.; Friend, R. H. *Nature* **2005**, *434*, 194.
(83) Horowitz, G.; Bachet, B.; Yassar, A.; Lang, P.; Demanze, F.; Fave, J.-L.; Garnier, F. *Chem. Mater.* **1995**, *7*, 1337.
(84) Facchetti, A.; Letizia, J.; Yoon, M.-H.; Mushrush, M.; Katz, H. E.; Marks, T. J. *Chem. Mater.* **2004**, *16*, 4715.
(85) Facchetti, A.; Yoon, M.-H.; Stern Charlotte, L.; Hutchison Geoffrey, R.; Ratner Mark, A.; Marks Tobin, J. *J. Am. Chem. Soc.* **2004**, *126*, 13480.
(86) Kim, S.-J.; Lee, Y.-J.; Kang, E.; Kim, S. H.; Ko, J.; Lee, B.; Cheong, M.; Suh, I.-H.; Kang, S. O. *Organometallics* **2003**, *22*, 3958.
(87) Kotlar, A. J.; Kriner, W. A.; Mueller, T. E.; Falvello, L. R. *Polyhedron* **1996**, *15*, 1545.
(88) Daiss, J. O.; Penka, M.; Burschka, C.; Tacke, R. *Organometallics* **2004**, *23*, 4987.
(89) Garnier, F.; Hajlaoui, R.; El Kassmi, A.; Horowitz, G.; Laigre, L.; Porzio, W.; Armanini, M.; Provasoli, F. *Chem. Mater.* **1998**, *10*, 3334.
(90) Kim, D.-H.; Ohshita, J.; Lee, K.-H.; Kunugi, Y.; Kunai, A. *Organometallics* **2006**, *25*, 1511.
(91) Frisch, M. J.; Trucks, G. W.; Schlegel, H. B.; Scuseri, G. E.; Robb, M. A.; Cheeseman, J. R.; Montgomery, J. A. Jr.; Vreven, T.; Kudin, K. N.; Burant, J. C.; Millam, J. M.; Iyengar, S. S.; Tomasi, J.; Barone, V.; Mennucci, B.; Cossi, M.; Scalmani, G.; Rega, N.; Petersson, G. A.; Nakatsuji, H.; Hada, M.; Ehara, M.; Toyota, K.; Fukuda, R.; Hasegawa, J.; Ishida, M.; Nakajima, T.; Honda, Y.; Kitao, O.; Nakai, H.; Klene, M.; Li, X.; Knox, J. E.; Hratchian, H. P.; Cross, J. B.; Adamo, C.; Jaramillo, J.; Gomperts, R.; Stratmann, R. E.; Yazyev, O.; Austin, A. J.; Cammi, R.; Pomelli, C.; Ochterski, J. W.; Ayala, P. Y.; Morokuma, K.; Voth, G. A.; Salvador, P.; Dannenberg, J. J.; Zakrzewski, V. G.; Dapprich, S.; Daniels, A. D.; Strain, M. C.; Farkas, O.; Malick, D. K.; Rabuck, A. D.; Raghavachari, K.; Foresman, J. B.; Ortiz, J. V.; Cui, Q.; Baboul, A. G.; Clifford, S.; Cioslowski, J.; Stefanov, B. B.; Liu, G.; Liashenko, A.; Piskorz, P.; Komaromi, I.; Martin, R. L.; Fox, D. J.; Keith, T.; Al-Laham, M. A.; Peng, C. Y.; Nanayakkara, A.; Challacombe, M.; Gill, P. M. W.; Johnson, B.; Chen, W.; Wong, M. W.; Gonzalez, C.; Pople, J. A. *Gaussian 03, revision D.02*; Gaussian Inc.: Wallingford, CT, 2004.
(92) Becke, A. D. *J. Chem. Phys.* **1993**, *98*, 1372.
(93) Francl, M. M.; Pietro, W. J.; Hehre, W. J.; Binkley, J. S.; Gordon, M. S.; DeFrees, D. J.; Pople, J. A. *J. Chem. Phys.* **1982**, *77*, 3654.
(94) Runge, E.; Gross, E. K. U. *Phys. Rev. Lett.* **1984**, *52*, 997.
(95) Gross, E. K. U.; Kohn, W. *Adv. Quantum Chem.* **1990**, *21*, 255.
(96) Gross, E. K. U.; Ullrich, C. A.; Gossman, U. J. *In Density Functional Theory*; Gross, E. K. U., Driezler, R. M., Eds. Plenum Press: New York, 1995; p 149.
(97) Casida, M. E. In *Recent Advances in Density Functional Methods*; Chong, D. P., Ed.; World Scientific: Singapore, 1995; Part 1, p 115.